

Watershed-scale provenance heterogeneity within Eocene nonmarine basin fill: Southern Greater Green River Basin, western USA

Ethan C. Parrish^{1,†}, Alan R. Carroll¹, Holly Gregorich², M. Elliot Smith², and Colby Schwaderer¹

¹Department of Geoscience, University of Wisconsin–Madison, 1215 West Dayton Street, Madison, Wisconsin 53715, USA ²School of Earth Sciences and Environmental Sustainability, Northern Arizona University, Flagstaff, Arizona 86011, USA

ABSTRACT

Weathering, erosion, and sediment transport in modern landscapes may be investigated via direct observation of attributes such as elevation, relief, bedrock lithology, climate, drainage organization, watershed extent, and others. Studies of ancient landscape evolution lack this synoptic perspective, however, and instead must rely more heavily on downstream records of fluvial deposits. Provenance analysis based on detrital grain ages has greatly enhanced the utility of such records but has often focused broadly on regional to continental scales. This approach may overlook important details of localized watersheds, which could lead to significant misinterpretation of past sediment dispersal patterns. The present study, therefore, explores the impact of geographic and stratigraphic sampling density on detrital zircon provenance, based on a high-density investigation of U-Pb ages (N = 23, n = 4905)obtained from a narrow chronostratigraphic range (\sim 2 m.y.) within a relatively small $(\sim 25,000 \text{ km}^2)$ area of an Eocene nonmarine sedimentary basin. Based on multidimensional scaling and DZmix modeling, these strata comprise seven distinct, approximately isochronous detrital zircon (DZ) chronofacies, defined as "... a group of sedimentary rocks that contains a specified suite of detrital zircon age populations" (Lawton et al., 2010). Four of these DZ chronofacies reflect long-distance transport from extrabasinal source areas. DZ chronofacies CO-1 and CO-2 are interpreted to derive from a primary sediment source in central Colorado (USA), corroborating previously proposed long-distance sediment transport via the Aspen paleoriver. DZ chronofacies ID-1 and ID-2 are interpreted to have been deliv-

Alan R. Carroll **b** https://orcid.org/0000-0002

†eparrish3@wisc.edu

GSA Bulletin; published online 5 September 2023

ered to the basin from central Idaho by the Idaho paleoriver. In contrast, DZ chronofacies UT-1 and UT-2 are interpreted to reflect local drainage from the Uinta Uplift south of the basin, and DZ chronofacies WY-1 is interpreted to have been sourced from the Rawlins, Granite, and Sierra Madre uplifts to the north and east via the Toya Puki paleoriver. Lateral transitions between different DZ chronofacies in some cases occur over distances as little as 5 km, implying that depositional systems carrying sand from disparate watersheds directly competed to fill available basin accommodation. The results of this study reveal a high degree of complexity of Eocene rivers that converged on the Greater Green River Basin, indicating that their deposits contain a rich record of finescale landscape evolution across much of the Laramide foreland and Cordilleran orogen. These results illustrate the need for adequate sample density when assessing basin-scale provenance and offer a cautionary consideration for researchers using sandstone (and incorporated authigenic cement) in other nonmarine basins as the basis for paleoaltimetry or detrital thermochronology studies.

INTRODUCTION

The weathering, erosion, and transport processes that shape modern continental landscapes and control the downstream delivery of weathering products shed light on a host of topics including, though not limited to, the influence of agriculture and bedrock lithology on streamdissolved organic carbon (e.g., Longworth et al., 2007; Stahl et al., 2021), differential silicate weathering fluxes based on bedrock lithology and land use (e.g., West et al., 2002), pre-versus post-development denudation rates (e.g., Brown et al., 1998), spatial differences in denudation rates (e.g., Norton et al., 2010; Zhao et al., 2015), changes in erosion rates following glacial retreat (e.g., Delaney et al., 2018) and sediment mixing processes across source-to-sink transects (e.g., Sickmann et al., 2016). Allogenic and autogenic influences on watershed evolution exert important controls on the nature of the downstream deposits (e.g., Zhao et al., 2015; Romans et al., 2016; Sickmann et al., 2016). Conversely, basinal deposits can provide a record of the geomorphic processes active upstream (e.g., Wren and Davidson, 2011).

The advent of rapid and inexpensive radioisotopic analyses of detrital zircon (DZ) grains (Gehrels, 2012, 2014) has revolutionized sedimentary provenance studies that link upstream processes to downstream products, and thus are profoundly expanding our understanding of source-to-sink relationships (e.g., Davis et al., 2010; Laskowski et al., 2013; Sickmann et al., 2016; Blum et al., 2017; Leary et al., 2020). U-Pb geochronology has been widely employed to document watershed- to sub-watershed-scale provenance heterogeneity in modern fluvial systems (e.g., Capaldi et al., 2017; Jackson et al., 2019). For example, DZ results from Ecuador reveal drastic downstream changes within a single watershed, as the Rio Pastaza traverses the Andean hinterland to the foreland (Jackson et al., 2019). In contrast, DZ studies of ancient fluvial systems are commonly more limited in their spatial resolution, with a focus on regional rather than watershed-scale variations (e.g., Rainbird et al., 2012; Laskowski et al., 2013; May et al., 2013; Gehrels and Pecha, 2014; Blum et al., 2017). Studies of ancient DZ provenance may also be hindered by limited chronostratigraphic control (e.g., Dickinson and Gehrels, 2003; Link et al., 2005; Sickmann et al., 2016; Karlstrom et al., 2018; Leary et al., 2020), which can make synoptic reconstruction of ancient drainage networks difficult to impossible.

Closed, nonmarine sedimentary basins offer an opportunity to better reconstruct detailed, synoptic source-to-sink relationships. Such basins can capture a relatively detailed and complete record of watershed- to sub-watershed-scale sediment delivery (e.g., Hinderer and Einsele, 2001; Smith et al., 2008; Allen and Allen, 2013), and interfingered lacustrine strata

https://doi.org/10.1130/B36822.1; 9 figures; 3 tables; 1 supplemental file.

can provide greatly improved chronostratigraphic control. Eocene fluvial deposits of the Greater Green River Basin in southwestern Wyoming (USA) represent an ideal test case for this approach, due to their excellent outcrop exposure, well-established lithostratigraphy (Smoot, 1983; Roehler, 1993; Pietras and Carroll, 2006; Smith et al., 2015), and extensive radioisotopic dating of volcanic tuffs deposited in Eocene paleolake Gosiute (Smith et al., 2003, 2008, 2010; Meyers, 2008; Aswasereelert et al., 2013; Machlus et al., 2015; Bruck et al., 2023). Past studies have inferred that detritus was supplied to the basin via intrabasinal (Smoot, 1983; Roehler, 1993), interbasinal (Dickinson et al., 1988), and orogen-scale rivers (Davis et al., 2010; Chetel et al., 2011; Hammond et al., 2019). Based on DZ age analyses of six existing samples (n = 861; Hammond et al., 2019) and 17 new samples (n = 4044), this study shows that at least four distinct watersheds contributed detritus to a relatively small (\sim 25,000 km²) area of the southeastern Green River Basin. Detrital zircon analyses based on geographically dense sampling are therefore vital to accurately interpret paleoelevation, paleoclimate, and sediment flux across the Laramide foreland.

GEOLOGIC SETTING

During the Late Cretaceous to early Paleogene, contractile tectonics within the North American Cordillera transformed the foreland landscape from a low-relief marine basin to the central Rocky Mountain region of North America (Fig. 1A; Weimer, 1960; Dickinson and Snyder, 1978; Bird, 1984, 1998; Dickinson et al., 1988; DeCelles, 2004). The final (70-50 Ma) phase of Cordilleran compression induced a series of diversely oriented and segmented, anticlinal basement-cored uplifts and associated basins across the foreland (Fig. 1A; DeCelles, 2004; Ersley, 1988). These basins acted as sediment sinks for several large and dynamically evolving watersheds (e.g., Dickinson et al., 1988; Carroll et al., 2006; Smith et al., 2014; Lawton, 2019). Several regional-scale paleorivers have been proposed as inputs to lakes that occupied the Uinta, Piceance, and Greater Green River basins, including the Idaho River (Chetel et al., 2011), California River (Davis et al., 2010), Aspen River (Smith et al., 2014; Hammond et al., 2019), and the Toya Puki River (this study).

The Greater Green River Basin comprises the Bridger, Washakie, Great Divide, and Sand Wash sub-basins, and is bounded by the Sevier fold and thrust belt to the west, the Wind River and Granite Mountains to the north, the Rawlins Uplift and Sierra Madre Mountains to the east, and the Uinta Mountains to the south (Fig. 1; Love et al., 1963). Sub-basins comprising the Greater Green River Basin are separated by anticlinal structures including the Rock Springs Uplift, Wamsutter Arch, and Cherokee Ridge (Fig. 1B; Roehler, 1992; Jesse et al., 2011).

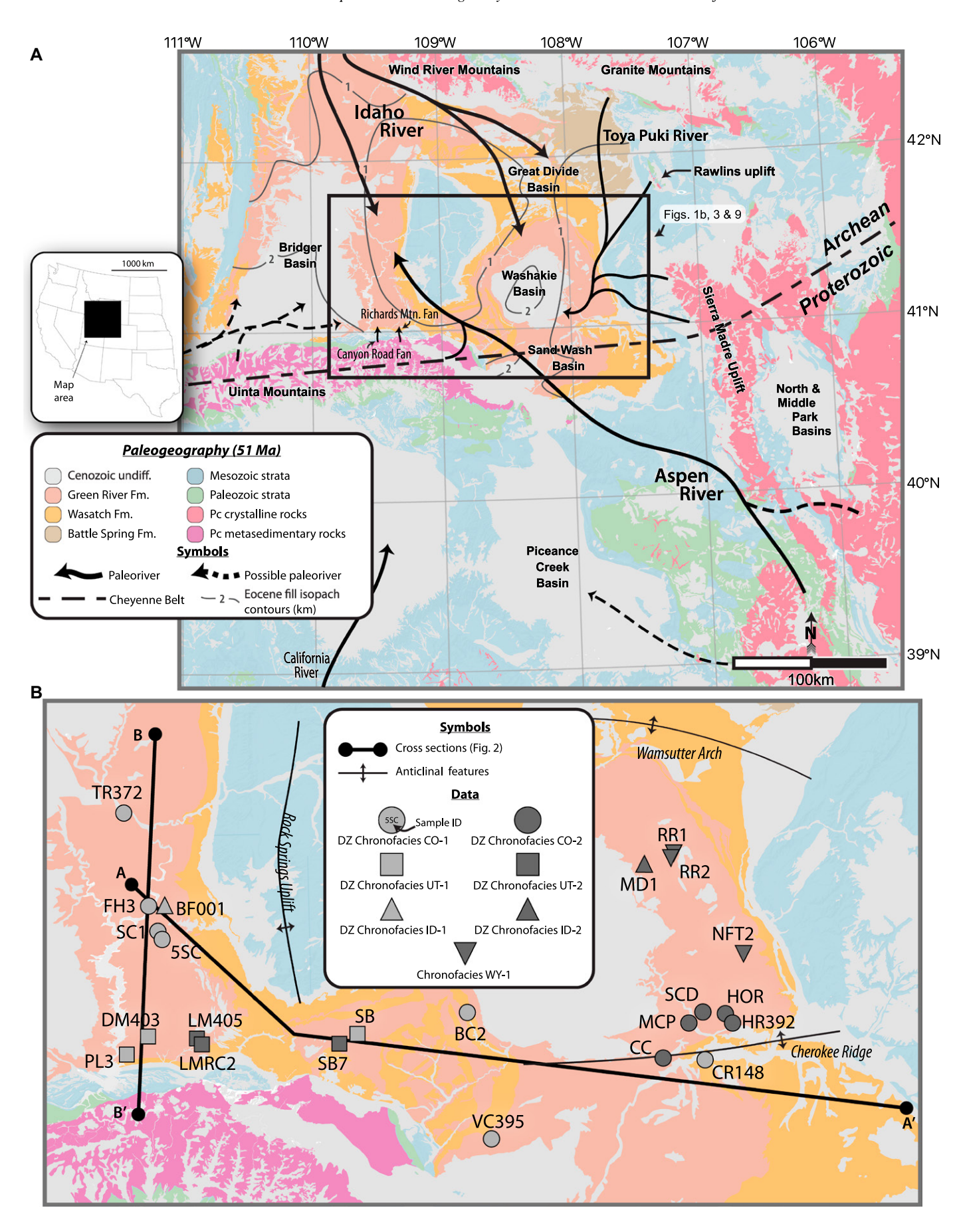
While each sub-basin records a unique succession of strata, the long-term trend in each is an evolution from a hydrologically open to closed system, followed by a return to a hydrologically open system during deposition of the Green River Formation between ca. 53.5 Ma and ca. 48.5 Ma (Fig. 2; Roehler, 1969, 1992; Carroll and Bohacs, 1999; Smith et al., 2003, 2008, 2010; Machlus et al., 2015). Specifically, the Luman Tongue, Tipton, Wilkins Peak, and Laney Members of the Green River Formation record a progression from fluvial to fluvial-lacustrine to fluctuating profundal to evaporative lacustrine and back (Fig. 2). The evaporative Wilkins Peak Member is primarily limited to the Bridger sub-basin and is laterally equivalent to alluvial deposits of the Cathedral Bluffs Member of the Wasatch Formation in the adjacent Washakie, Great Divide, and Sand Wash sub-basins (Fig. 2; Bradley, 1964; Sullivan, 1985; Roehler, 1992). The Laney Member overlies the Wilkins Peak Member and records an expansion of lacustrine strata into all the sub-basins of the Greater Green River Basin (Fig. 2; Surdam and Stanley, 1980; Roehler, 1992). Alluvial, volcaniclastic sediment of the Sand Butte bed of the Laney Member records a time-transgressive replacement of lacustrine strata in the Greater Green River Basin from north to south (Fig. 2; Roehler, 1992).

The Greater Green River Basin straddles the W-SW- to E-NE-trending Cheyenne Belta regional suture that juxtaposes the Archean Wyoming province to the north with interpreted Proterozoic magmatic arc and related rocks of the Yavapai-Mazatzal province to the south (Fig. 1A; Karlstrom and Houston, 1984; Templeton and Smithson, 1994). The Cheyenne Belt is exposed in the Sierra Madre, Medicine Bow, and Laramie uplifts, of which the Laramie represent the easternmost exposure of the Cheyenne Belt (Karlstrom and Houston, 1984). Nd-isotope and trace element data of sediment from the Neoproterozoic Uinta Mountain Group suggest its derivation from the Wyoming province to the north and from a westward-flowing fluvial system sourcing younger sediments from the East (Ball and Farmer, 1998). Ball and Farmer (1998) suggest that the Uinta Mountain Group and the modern Uinta Mountains roughly represent the southern edge of the Wyoming province and the linear extent of the Cheyenne Belt reactivated before subsequent Cenozoic contraction. Prominent uplifts surrounding the basin exhumed sediment sources that include widespread Paleozoic passive margin strata, Cretaceous foreland basin Figure 1. (A) Generalized paleogeographic map (51 Ma) showing locations of principal Laramide uplifts and Eocene paleocatchment of the Greater Green River and surrounding basins in the western USA. Isopach thicknesses for Eocene fill are shown with 1 km counters (after Smith et al., 2008). Additionally depicted are the Cheyenne Belt, alluvial fans (Smith et al., 2015), as well as known and proposed paleodrainage paths. (B) Map of field area showing detrital zircon sample locations by detrital zircon (DZ) chronofacies (see discussion) and cross-section locations (Fig. 2). Fm.— Formation; Mtn.—Mountain; Pc—Precambrian: undiff.—undifferentiated.

deposits, and Late Cretaceous to Paleogene magmatism ranging from the Colorado Mineral Belt in central Colorado to the Challis and Absaroka volcanics of central Idaho and northwest Wyoming (Bookstrom, 1989, 1990; DeCelles, 2004; Dickinson and Gehrels, 2008; Chetel et al., 2011; Chapin, 2012; Laskowski et al., 2013; Fayon et al., 2017).

METHODS

Field investigations were predominantly carried out on fluvial outcrops of the Wilkins Peak Member on the south and east margins of the Bridger sub-basin and directly south of the Rock Springs Uplift, as well as on age-equivalent fluvial outcrops on the western and eastern margins of the Washakie and Great Divide sub-basins (Figs. 1–3). This study is based on a total of 52 fluvial sandstone samples, six from Hammond et al. (2019), plus 46 new samples. Of the 46 new samples, 42 have associated petrographic data and 18 have associated DZ data (Table 1). New samples were collected from 17 fluvial outcrop localities within the Wasatch and Green River formations in the southern and eastern reaches of the Greater Green River Basin (Figs. 1-3). A total of 303 new paleocurrent indicators were measured across six localities within the Wilkins Peak and Cathedral Bluffs members within the Bridger and Washakie sub-basins (Fig. 3). For all localities, trough cross-bedding was measured, and in one locality (associated with sample SB3 18) lateral accretionary faces were also measured (Fig. 3). Point counts of sandstone framework grains were conducted using a modified Gazzi-Dickinson method (Ingersoll et al., 1984). Framework grains not considered include phyllosilicates, accessory minerals, dense minerals, and unidentified grains. Samples for petrographic analysis range from very fine- to very coarse-grained fluvial sandstones from 15 out-



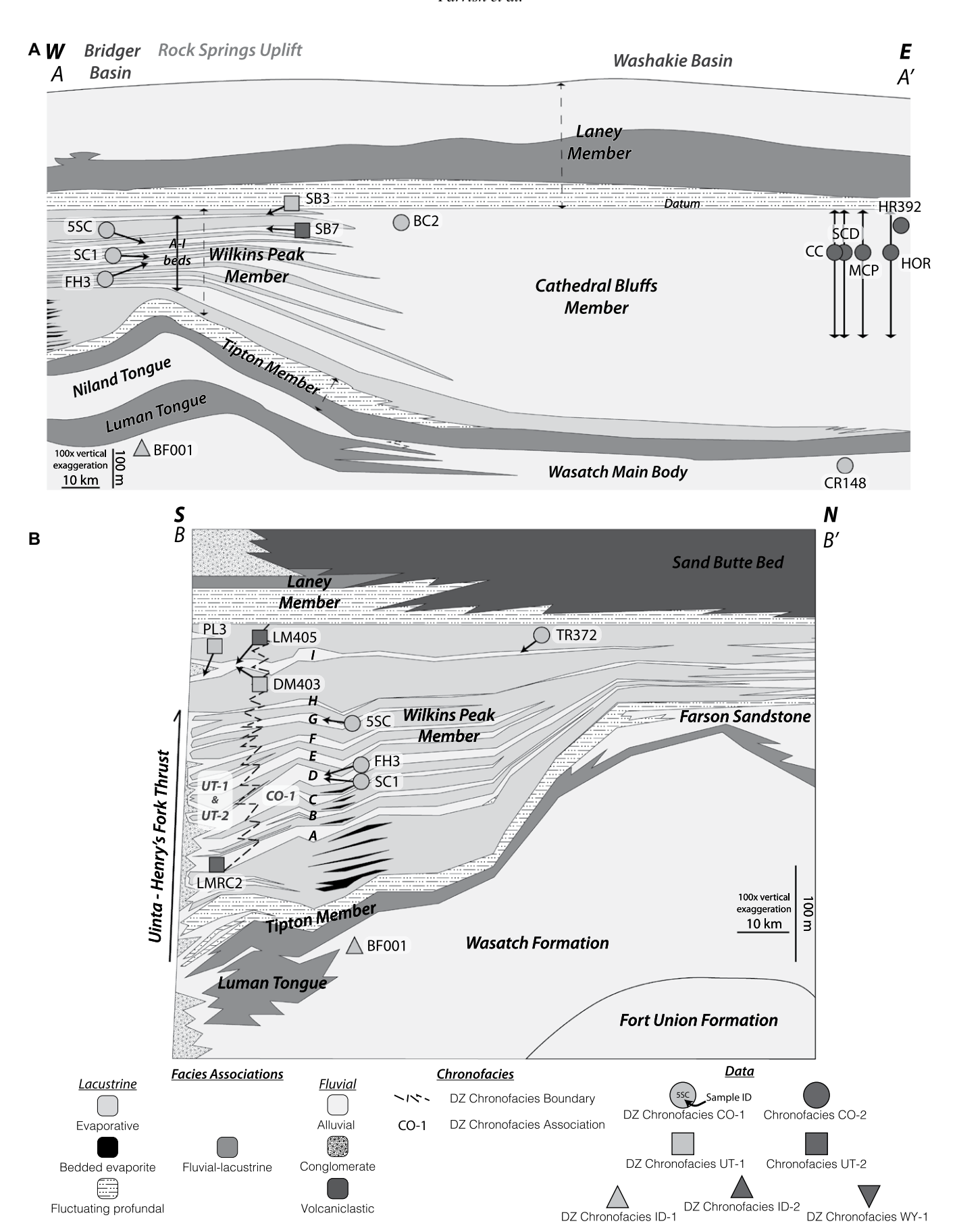


Figure 2. (A) Schematic east-west cross section along the axis of the Aspen paleoriver (present-day western USA) modified from Smith et al. (2015). A–I beds indicate named alluvial horizons of Culbertson (1961). Sample locations (this study and Hammond et al., 2019) are organized by detrital zircon (DZ) chronofacies (see discussion). Error bars associated with samples CC, SCD, MCP, and HOR represent the precision of stratigraphic location for samples collected by Hammond et al. (2019). (B) Schematic N-S cross section modified from Smith et al. (2015). Sample locations (this study) are organized by DZ chronofacies (Fig. 7).

crop localities (Fig. 3). Sandstone modal compositions were determined by counting 300+ total points per slide including porosity, matrix, and cement, for 42 of 43 thin sections (Table S1 in the Supplemental Material¹). Each thin section

'Supplemental Material. Table S1: Petrographic point counting data was gathered using a modified Gazzi-Dickinson point counting methodology. Table S2: U-Pb data for all samples from this study. Table S3: Paleocurrent data. Figures S1 and S2: Shepard plots for MDS analysis. Table S4: Sample results for DZmix modeling. Text S1: Pertinent detrital zircon provenance populations. Please visit https://doi.org/10.1130/GSAB.S.23638845 to access the supplemental material, and contact editing@geosociety.org with any questions.

was dual-stained with barium chloride + rhodizonate, as well as sodium cobaltinitrite, to distinguish potassium and plagioclase feldspar, respectively.

Detrital zircons were separated from 18 samples using standard separation techniques to prevent sample biases (e.g., grain size, shape, color, rounding) during separation (Sircombe and Stern, 2002; Fedo et al., 2003; Gehrels, 2012). Samples were first crushed in a jaw-crusher before being reduced to sand ($<\sim$ 2 mm) by a disc mill. Thereafter the sample was sieved to isolate grains between 125 μ m and 500 μ m. To separate the zircon grains, the isolated sample was first separated from lower-density minerals by gold-table density separation, from magnetic

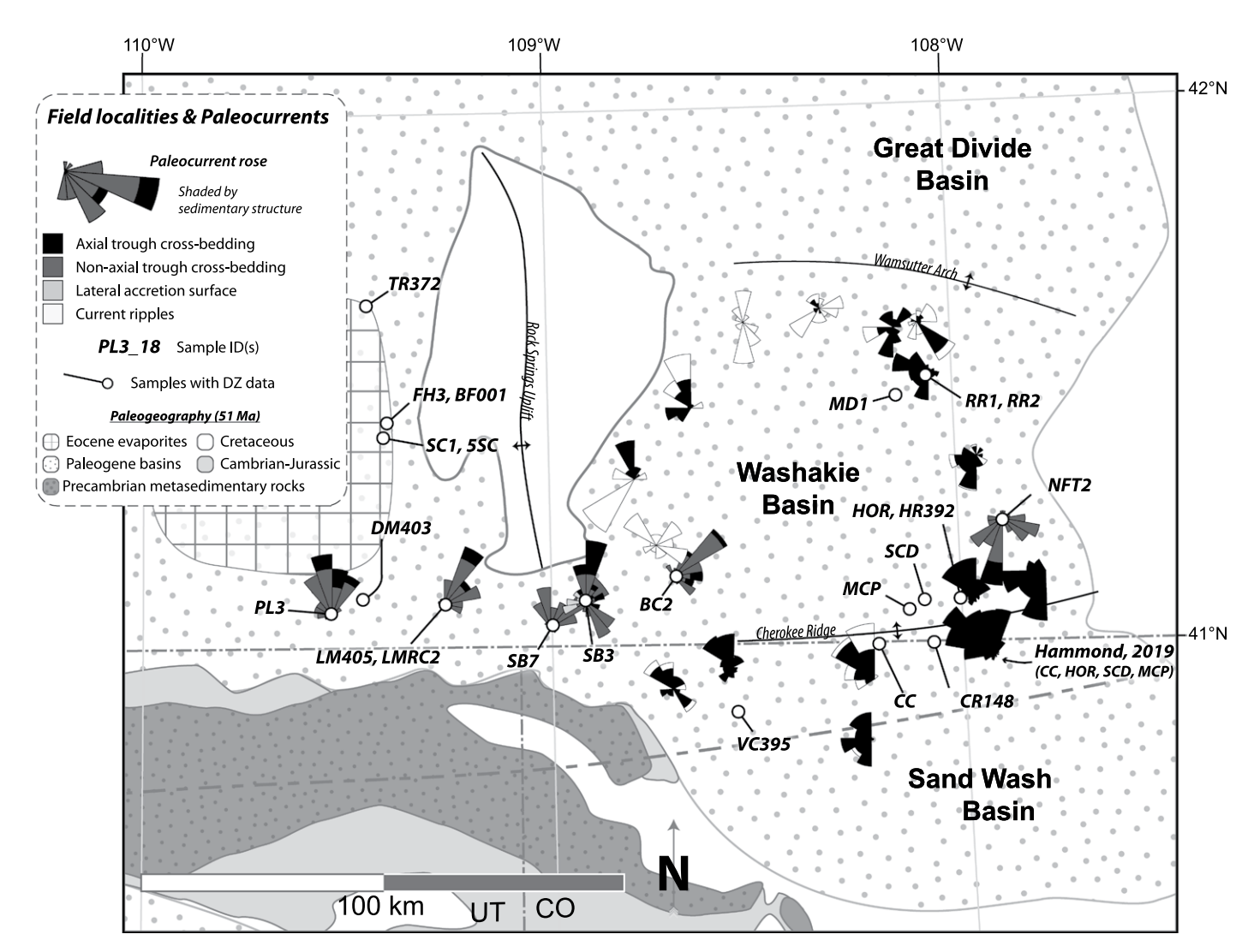


Figure 3. Detrital zircon (DZ) sample localities and paleocurrent data. Paleocurrent rose diagrams summarize the direction of reported measurements—a total of 303 from this study plus an existing 354 from Hammond et al. (2019) and 726 from Forss (1983)—subdivided by sedimentary structure (Fig. 3; Table S3 [see text footnote 1]). Pertinent structures, including the Rock Springs Uplift, the Wamsutter Arch, and the Cherokee Ridge (southwestern Wyoming, USA), are shown.

TABLE 1. DETRITAL ZIRCON SAMPLES (SOUTHWESTERN WYOMING, USA)

												U-Pb MDA	MDA*						
					ź	YSG§	YSG_ Ma	YSG_ Ma	YC2_ Ma#	YC2_ Ma	YC2_ Ma	YC2 MSWD	YC2 cluster	YC3_ Ma**	YC3_ Ma_	YC3_ Ma_	YC3 MSWD	YC3 cluster	No. of
Sample name	Abbreviated name	Latitude (°N)	Longitude (°W)	Member	⊃8		(± α	(± β 2α)		(± α	(± β		size		$(\pm \alpha 2\sigma)$	(± β 2α)		size	disc. grains
This study																			!
17-BF-001	BF001	41.3527	109.3339	Wasatch	82	73.02	0.78	1.02	73.76	0.48 1.48	0.82	0.78	ကျ	74.21	0.43	0.79	1.93	4 -	5 [
19-DM-403 19-HB-392	UM403	41.0724	109.479		9 1	153.27	7.7.2	98.00	307.45	20.0 20.0 20.0	3.84	0.57	ນ 4	304.87	20.0	2.7	0 iv	4 Œ	ວວ
19-LM-405	LM405	41.0771	109.3096	WPM	165	918.94	14.10	17.85	931.28	11.46	15.94	0.03	- ო	962.83	5.84	12.87	1.64	o ග	37
19-VC-395	VC395	40.8555	108.5031	CBM	195	48.27	0.43	0.63	55.61	0.32	0.62	0.63	2	56.19	0.22	0.58	1.97	2	2
5-SC_18	5SC	41.2899	109.3996	WPM	270	55.1	09.0	92.0	55.95	0.29	0.56	1.99	7	56.44	0.37	0.61	1.28	4	13
BC2_18	BC2	41.1164	108.5597	CBM	276	26.0	0.80	96.0	56.75	0.54	0.79	0.54	2	57.19	0.30	0.65	1.41	7	31
LMRC2_18	LMRC2	41.068	109.2854	WPM	278	307.8	0.70	2.96	403.82	0.38	3.79	0.81	7	995.60	5.61	10.87	1.12	우	36
MD1_20	MD1	41.4096	108.056	Laney	251	35.11	0.94	1.05	41.72	0.32	0.64	0.18	က	42.20	0.26	0.62	1.75	2	Ä. Ä.
NFT2_18	NFT2	41.2245	107.8093	CBM	293	2.69	1.00	1.17	86.69	99.0	0.89	0.14	7	71.95	0.30	69.0	1.57	F	8
PL3_18	PL3	41.0339	109.5227	WPM	223	49.7	4.40	4.43	330.37	4.67	5.62	0.07	7	326.19	3.65	4.79	2.83	ო	4
RR1_20	RR1	41.4334	107.9935	CBM	262	45.49	0.68	98.0	90.61	0.59	1.20	0.82	က	91.84	0.44	1.15	2.46	9	Ä. Ä.
RR2_20	RR2	41.4334	107.9945	Laney	267	41.88	1.81	1.90	56.52	1.51	1.68	1.69	7	75.55	69.0	1.21	1.65	œ	Ä. Ä.
SB3_18	SB3	41.0773	108.8638	WPM	296	57.0	1.00	1.08	57.35	99.0	0.77	0.21	4	57.90	0.30	0.51	1.21	9	8
SB7_18	SB7	41.0605	108.9126	WPM	580	447.7	3.50	4.53	932.59	2.67	9.73	0.14	9	941.07	09.9	8.95	1.00	7	31
SC1_18	SC1	41.2899	109.3996	WPM	301	50.2	2.60	5.62	55.71	7.53	7.55	0.93	N	56.41	0.42	0.64	1.69	4	13
TR-19-372	TR372	41.5424	109.4822	WPM	178	50.61	0.59	0.77	51.11	0.33	0.60	0.67	က	51.11	0.33	0.60	0.67	ო	25
Hammond et al., 2019																			
CC-16	ပ္ပ	41.01033	108.0272	CBM	13	54.78	1.05	1.52	55.37	0.79	1.36	0.76	N	57.27	0.48	1.24	2.04	9	ď.
CR-148-16	CR148	41.00566	107.923	CBM	118	57.49	1.22	1.68	58.64	0.73	1.38	0.63	4	58.64	0.59	1.31	0.63	4	ď. Z
FH3_18	딾	41.3515	109.413	WPM	594	55.3	0.70	1.31	55.98	0.35	1.17	0.45	7	56.37	0.24	1.15	0.93	F	Ą. Z
HOR-16	HOH	41.09575	107.8637	CBM	106	56.17	1.24	1.67	57.07	0.36	1.20	0.58	ო	57.69	0.62	1.31	1.25	4	Ä.
MCP-16	MCP	41.08605	107.9454	CBM	118	55.04	- -	1.56	56.03	0.68	1.31	69.0	က	57.43	0.35	1.20	0.68	15	Ä. Z
SCD-16	SCD	41.09517	107.9292	CBM	112	26.37	1.14	1.60	57.61	0.59	1.29	0.38	=	57.89	0.33	121	0.76	೮	Y.A
Note: Bolded values represent accepted ages (e.g., Dickinson and G	epresent acce	oted ages (e	.g., Dickinsor	n and Gehrels,		2009b); MDA-	maximu	n deposi	-maximum depositional age;	Disc.	—discordant; YSG	nt; YSG—	youngest	single grain; YC2	iin; YC2-	-younge	youngest cluster	of two or r	more

grain ages (n ≥ 2); YC3—youngest cluster of three or more grain ages (n ≥ 3); MSWD—mean square of weighted deviates; WPM—Wilkins Peak Member; CBM—Cathedral Bluffs Member; N.A.—not applicable

Number of analyses

n grain age. ore grain ages (n \geq 2) overlapping in age at 1 σ . more grain ages (n \geq 3) overlapping in age at 2 §Youngest single detrital zircon #Youngest cluster of two or mor

higher-density minerals using a Franz magnetometer, then from light minerals using methylene iodide heavy liquids separation. U-Pb ages were determined for a target of \sim 315 grains per sample using laser ablation-inductively coupled plasma-mass spectrometry at the Arizona Laser-Chron Center at the University of Arizona (Tucson, Arizona, USA) (Gehrels et al., 2008; Gehrels and Pecha, 2014; Pullen et al., 2014, 2018). Data reduction was performed using the Arizona LaserChron Center's "AgeCalc" program (described in Gehrels and Pecha, 2014). Default discordance and reverse discordance filters of 20% and 5%, respectively, were applied to all samples (this study). Complete U-Pb analytical data is included in the Supplemental Material (Table S2).

Maximum depositional ages (MDAs) were calculated by three different metrics: "YSG" (youngest single grain age), "YC2" (youngest cluster of two or more grain ages ($n \ge 2$) overlapping in age at 1σ), and "YC3" (youngest cluster of three or more grain ages ($n \ge 3$) overlapping in age at 2σ) (e.g., Dickinson and Gehrels, 2009b) using the Python-based detrital-zircon analysis package "detritalPy" (Sharman et al., 2018; Table 1). Reported MDA uncertainties include both a MDA date uncertainty (a) and a total uncertainty (β) (Table 1). External uncertainties (Table S2) have been manually propagated with date uncertainties (α) into the total uncertainty (B) via quadrature and converted to Ma. For MDAs <900 Ma, the ²⁰⁶Pb/²³⁸U external uncertainty was used. For MDAs >900 Ma, the ²⁰⁶Pb/²⁰⁷Pb external uncertainty was used. For samples from Hammond et al. (2019), 2% external uncertainties were used (e.g., Horstwood et al., 2016).

We utilize both multi-dimensional scaling (MDS) (Vermeesch, 2013, 2018) and DZmix quantitative modeling (Sundell and Saylor, 2017) to assess statistical similarities and differences between samples. MDS is a dimension reduction statistical test that measures pairwise dissimilarity between two or more samples by calculating the Euclidean distance between samples. MDS plots were generated using DZmds (Saylor et al., 2018) for two compiled age ranges: 0-3500 Ma and 0-300 Ma. Two age ranges are shown to illustrate sample groupings more clearly and to remove the homogenizing influence of older ages for samples more appropriately compared according to their younger age populations. For all MDS analyses, kernel density estimate (KDE) distributions with adaptive bandwidth algorithms were used, stress was calculated and minimized using the metric squared criterion and the comparison statistics were chosen based on the best (lowest) Shepard plot stress value for three dimensions. Where MDS is purely a statistical test of sample similarity that avoids a priori assumptions about zircon sources, DZmix seeks to determine mixing proportions from potential sources through inverse Monte Carlo modeling, wherein mixed samples are compared to randomly generated combinations of source distributions, and a range of best mixing proportions are retained (Sundell and Saylor, 2017). For all DZmix models, cross-correlation comparison metrics were used. For the 0-300 Ma DZmix models a KDE density distribution with a fixed 1 m.y. bandwidth was used, and for the 0-3500 Ma models KDE density distributions with optimized bandwidths were used. In both age models, Monte Carlo simulations were run 15,000 times for each sample (Sundell and Saylor, 2017).

Source compilations include U-Pb ages measured from in situ and detrital grains in the Sierra Madre Mountains, Uinta Mountains, and the Colorado Mineral Belt as well as detrital grains associated with the Rawlins Uplift in south-central Wyoming (Premo and Van Schmus, 1989; Souders and Frost, 2006; Dehler et al., 2010; Klein et al., 2010; Lynds and Xie, 2019). For the Colorado Mineral Belt, source compilations also include ages obtained via K-Ar and 40Ar/39Ar chronometers (Klein et al., 2010). Both MDS and DZmix models were employed to more reliably characterize sample similarity. To further corroborate MDS and DZmix outputs, petrographic, MDA, and paleocurrent data were then compared on a sample-by-sample basis.

RESULTS

Paleocurrents

Paleocurrent directions vary across the Greater Green River Basin (Fig. 3). Figure 3 summarizes paleocurrent data collected as part of this study in addition to existing data published by Forss (1983) and Hammond et al. (2019). Paleocurrent trends can be grouped into three general groups: paleocurrents indicating north to northeastward paleoflow (N = 5), paleocurrents indicating a predominantly northwestward paleoflow (N = 9), and paleocurrents indicating southeast to southwestward paleoflow (N = 7) (Fig. 3). Complete paleocurrent data is included in the Supplemental Material (Table S3).

Sandstone Petrography

Framework grain compositions were determined by point counting, using a modified Gazzi-Dickinson method (Ingersoll et al., 1984). Of 42 sandstone samples analyzed, 25 are arkosic arenite, 12 subarkose, three sub-

lithic arenite, and two are quartz arenite (modified Dott, 1964; Fig. 4). More mature samples (quartz arenites, subarkoses, and sublithic arenites) occur adjacent to the Uinta Uplift, whereas less mature samples (arkosic arenites) occur farther from the Uintas (Fig. 3). There are two exceptions to this general trend. First, two of the six samples adjacent to the Uinta Uplift are arkosic arenite, while the remaining four are subarkose, sublithic arenite, or quartz arenite (Figs. 3 and 4). Second, despite the close geographic proximity of the three Scrivner Butte localities, they show distinct differences in mineralogic maturity. The three samples from Scrivner Butte_A are arkosic arenite, the two samples from Scrivner Butte_C are subarkose, and of the two samples from Scrivner Butte_B, one is arkosic arenite and the other subarkose. Finally, seritization of plagioclase feldspar was observed at several localities including Firehole Canyon, Sage Creek, Badger Creek, and Scrivner Butte_A (Fig. 5).

U-Pb Geochronology

For the 11 samples taken from the Wilkins Peak Member, U-Pb individual grain ages range from 46.2 Ma to 3551.1 Ma. For the 10 samples taken from the Cathedral Bluffs Member of the Wasatch Formation, U-Pb individual grain ages range from 45.5 Ma to 3215.2 Ma. Two samples were collected from the Laney Member, they range in age from 35.1 Ma to 2940.0 Ma. Sample 17-BF-001 was collected from the Wasatch Main Body Member and ranges in age from 73.0 Ma to 2957.7 Ma. Considering all samples (including Hammond et al., 2019), major detrital zircon age populations define multiple peaks ranging from the Paleogene to the Archean (Fig. 6A). For compiled source spectra, major detrital zircon age populations define peaks at ca. 1040 Ma, ca. 1090 Ma, and ca. 2660 Ma for the Uintas; ca. 1755 Ma and ca. 2650 Ma for the Sierra Madre; ca. 75 Ma, ca. 95 Ma, and ca. 1700 Ma for Rawlins Uplift; and ca. 65 Ma, with minor ca. 57 Ma and ca. 71 Ma peaks, as well as ca. 520 Ma, ca. 1370 Ma, and ca. 1700 Ma for the Colorado Mineral Belt. When divided by chronometer, age peaks for the Colorado Mineral Belt are ca. 1430 Ma and ca. 1700 Ma for U-Pb ages, and ca. 57 Ma, ca. 65 Ma, ca. 71 Ma, ca. 520 Ma, and ca. 1370 Ma for K-Ar and ⁴⁰Ar/³⁹Ar ages (Fig. 6).

Maximum depositional ages are reported in Table 1 and shown in Figure 6. Except for samples TR-19-372 and MD1_20, all calculated MDAs were at least 4 m.y. older than the ages indicated by lower bounding volcanic tuffs (Table 2; Smith et al., 2008, 2010).

Similarity Testing

For 0–300 Ma MDS analysis, a Shepard plot stress of 0.061912 was obtained using the cross-correlation comparison metric. For 0-3500 Ma MDS analysis, the youngest age for sample PL3_18 was omitted as an outlier, and a Shepard plot stress of 0.072596 was obtained using the cross-correlation comparison metric. Shepard plots are included in the Supplemental Material (Figs. S1 and S2).

DZmix model results returned poor crosscorrelation R-values (Table S4). For 0-3500 Ma models, R-values ranged from 0.336 ± 0.01 to 0.665 ± 0.004 , not including MD1_20, which we consider an outlier (discussed later). For 0-300 Ma models, R-values ranged from 0.168 ± 0 to 0.703 ± 0 (again omitting MD1_20). We believe this to be a function of the complexity of our samples and their variable sources, and attribute the poor DZmix fit values to insufficient source comparison data to reliably identify the complexities of our samples. Regardless, DZmix results are incorporated here as we believe they capture the influence of the four primary provenance sources across our data and are largely corroborated by MDS, petrographic, and paleocurrent analysis.

Figure 7 summarizes both MDS analysis and DZmix modeling for ages 0–3500 Ma (Fig. 7A) and 0–300 Ma (Fig. 7B). DZmix outputs are displayed as pie-plots, showing the modeled relative percentage of different provenance sources per sample, overlain on a MDS plot. DZ chronofacies associations (e.g., CO-1, CO-2, etc.) are based on MDS and DZmix outputs, as well as visual spectral analysis. Details of why certain samples are grouped in specific DZ chronofacies are discussed later.

Detrital Zircon Chronofacies

The distribution and magnitude of detrital zircon age populations in a sandstone represents an intrinsic rock property that is analogous to framework grain composition or heavy mineral assemblage. To describe this property Lawton et al. (2010) proposed the term "chronofacies," which they defined as "a group of sedimentary rocks that contains a specified suite of DZ age populations." It must be noted this term differs in meaning from the similar-sounding term "chronozone," which is formally defined as ". . . the body of rocks formed anywhere during the time span of some designated stratigraphic unit or geologic feature" (Murphy and Salvador, 1999). "Chronofacies" does not signify the age of rock formation, but instead the age distribution of included detrital zircon grains (note that the two terms may be equivalent in the case of a sand-

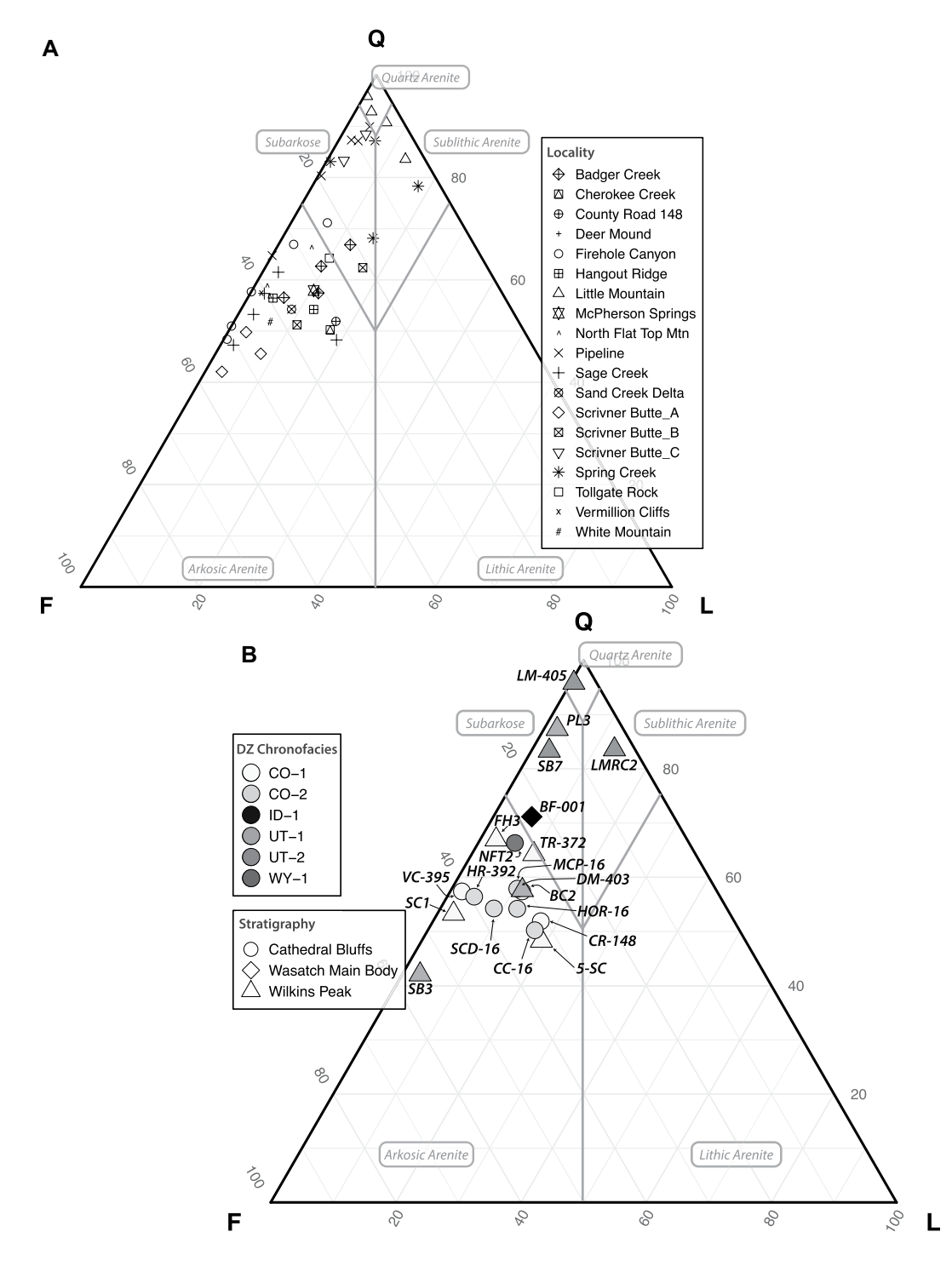


Figure 4. Sandstone ternary plots. **Q**—monocrystalline quartz + polycrystalline cluding chert); F-plagioclase feldspar + potassium feldspar; and L-all lithic fragments (excluding intrabasinal carbonate grains). (A) All samples (including Hammond et al., 2019) organized by locality (southwestern Wyoming, USA). (B) Samples with corresponding detrital zircon (DZ) ages (Fig. 6) shaded by detrital zircon chronofacies (Fig. 7) and shaped by stratigraphy (Fig. 2; Table 1).

stone containing only juvenile volcanic grains). Herein we use "DZ chronofacies" to help distinguish this from occasional earlier, dissimilar uses of "chronofacies" in other applications.

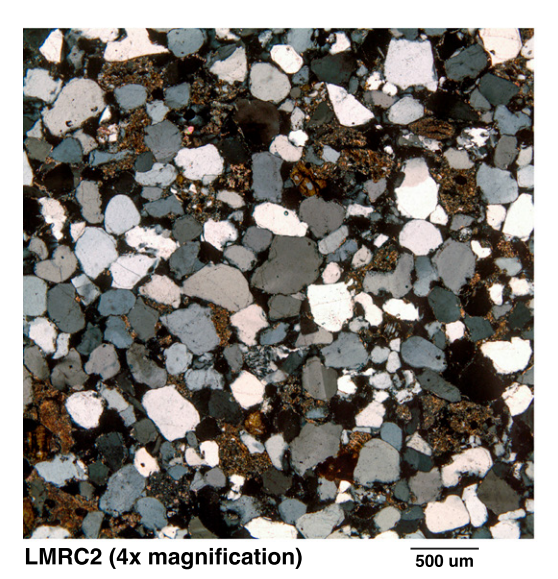
We identify seven distinct DZ chronofacies in this study: Colorado-1 (CO-1), Colorado-2 (CO-2), Utah-1 (UT-1), Utah-2 (UT-2), Wyoming-1 (WY-1), Idaho-1 (ID-1), and Idaho-2 (ID-2) (Figs. 6 and 7). DZ chronofacies are named for their interpreted source regions (see

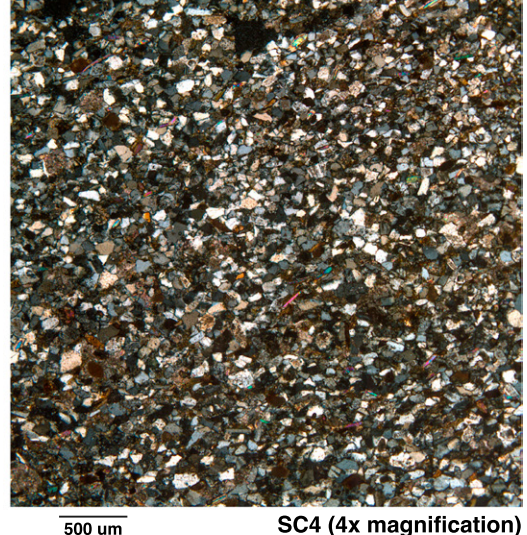
discussion), and, with the exception of sample SB3_18, these divisions are also reflected in calculated MDAs (Fig. 6; Table 1). Moreover, excepting samples in UT-1, these divisions are further recognized in sandstone framework grain compositions (Fig. 4B).

DZ Chronofacies CO-1 and CO-2

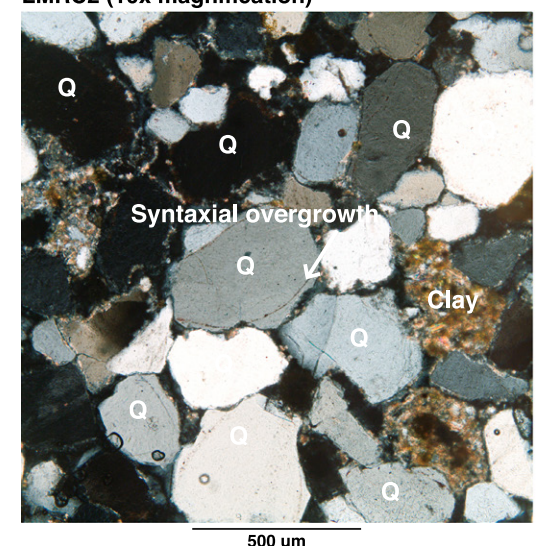
CO-1 characteristically features prominent Paleocene, mid-Mesoproterozoic, and late-

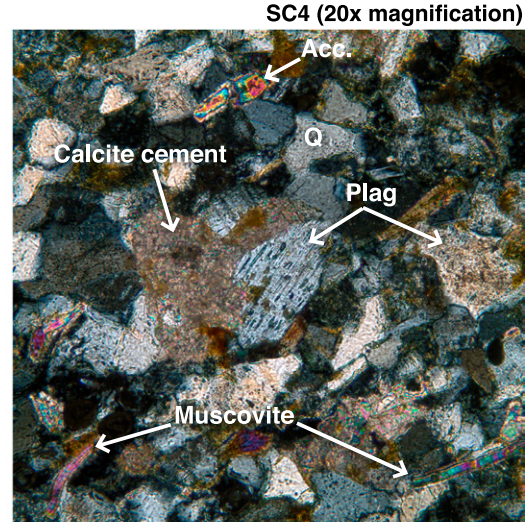
Paleoproterozoic age populations, as well as subdued Mesozoic, Paleozoic, and late-Mesoproterozoic populations. With the exception of sample TR-19-372 (discussed below), CO-1 has a notable dearth of Archean grains (Fig. 6A). CO-2 features the same prominent Paleocene, mid-Mesoproterozoic, and late-Paleoproterozoic age populations as well as the lack of Archean grains as CO-1, but lacks the subdued Mesozoic, Paleozoic, and late-Mesoproterozoic





LMRC2 (10x magnification)





500 um

CO-1 (right; primary Colorado Mineral Belt influence) (southwestern Wyoming, USA). Major differences include grain size and compositional maturity. Grains from CO-1 (SC4) are smaller and more arkose than those from UT-1 (LMRC2), which are larger and more quartz-rich. (Bottom) Magnified and annotated images of the same samples. Pervasive seritization (indicative of hydrothermal alteration) of plagioclase feldspars

is common in sands associated

with the Colorado Mineral Belt (DZ chronofacies CO-1 and CO-2). Acc.—accessory; Plag—plagioclase; Q—quartz.

Figure 5. (Top) Side-by-side comparison of sand indicative of detrital zircon (DZ) chronofacies UT-1 (left; primary Uinta influence) to DZ chronofacies

populations (Fig. 6A). For all but one sample (RR1_20, see discussion), MDS analysis clearly corroborates DZ chronofacies delineations (Fig. 7). Modeling of the relative contributions from the source domains using DZmix suggests that the majority of grains in CO-2 samples originated in central Colorado (Fig. 7). Samples in CO-1, however, are more variable, and DZmix modeling identifies age populations associated with all four source domains as significantly influencing these samples (Fig. 7).

Relative to DZ chronofacies UT-1 and UT-2, MDS analysis shows much greater inter-sample variation between samples in both CO-1 and CO-2 as well as in WY-1 (Fig. 7). Samples associated with CO-1 and CO-2 are all arkosic arenite (Fig. 4B) and all report MDAs of between 50 Ma and 58 Ma. (Fig. 6B; Table 1).

DZ Chronofacies UT-1 and UT-2

DZ chronofacies UT-1 and UT-2 contain large populations of late-Mesoproterozoic grains and more subdued populations of early-Mesoproterozoic ages. UT-1 additionally has subdued populations of Paleozoic and Paleoproterozoic grains. Both UT-1 and UT-2 contain small but present populations of Archean grains (Fig. 6A). With the exception of sample SB3_18 (discussed below), neither UT-1 nor UT-2 have any significant grain populations younger than Paleozoic in age. MDS analysis for both Utah DZ chronofacies indicates less inter-sample variation than Colorado or Wyoming DZ chronofacies (Fig. 7). Modeling with DZmix suggests that UT-2 is nearly exclusively derived from the Uinta Uplift whereas UT-1 also contains zircon grains derived from other sources (Fig. 7). Paleocurrent data for both UT-1 and UT-2 consistently indicate northward transport—away from the uplift (Fig. 3), and in both, sandstone grain size is generally coarser than in CO-1, CO-2, and WY-1 (e.g., Fig. 5).

Of the samples associated with UT-1 two are arkosic arenite and one subarkose (Fig. 4B). Of the three samples associated with UT-2, one is subarkose, another sublithic arenite, and the third is quartz arenite. With the exception of sample SB3_18 (discussed below), MDAs for UT-1 and UT-2 are all >300 Ma (Fig. 6A; Table 1).

DZ Chronofacies WY-1, ID-1, and ID-2

DZ chronofacies WY-1 contains Late Cretaceous, mid-Cretaceous, Paleoproterozoic, and Archean age populations as well as subdued Paleozoic, and early- and late-Mesoprotero-

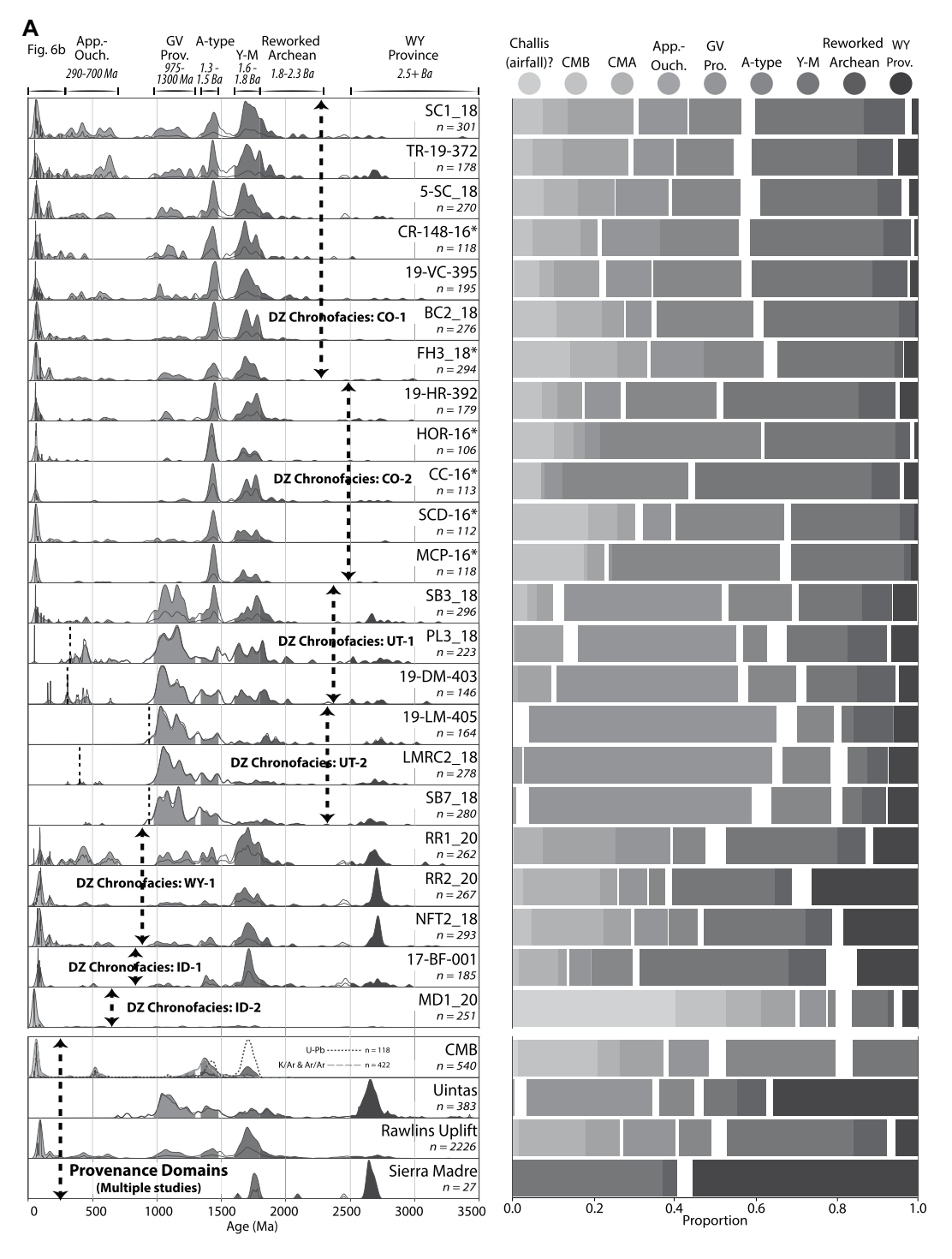


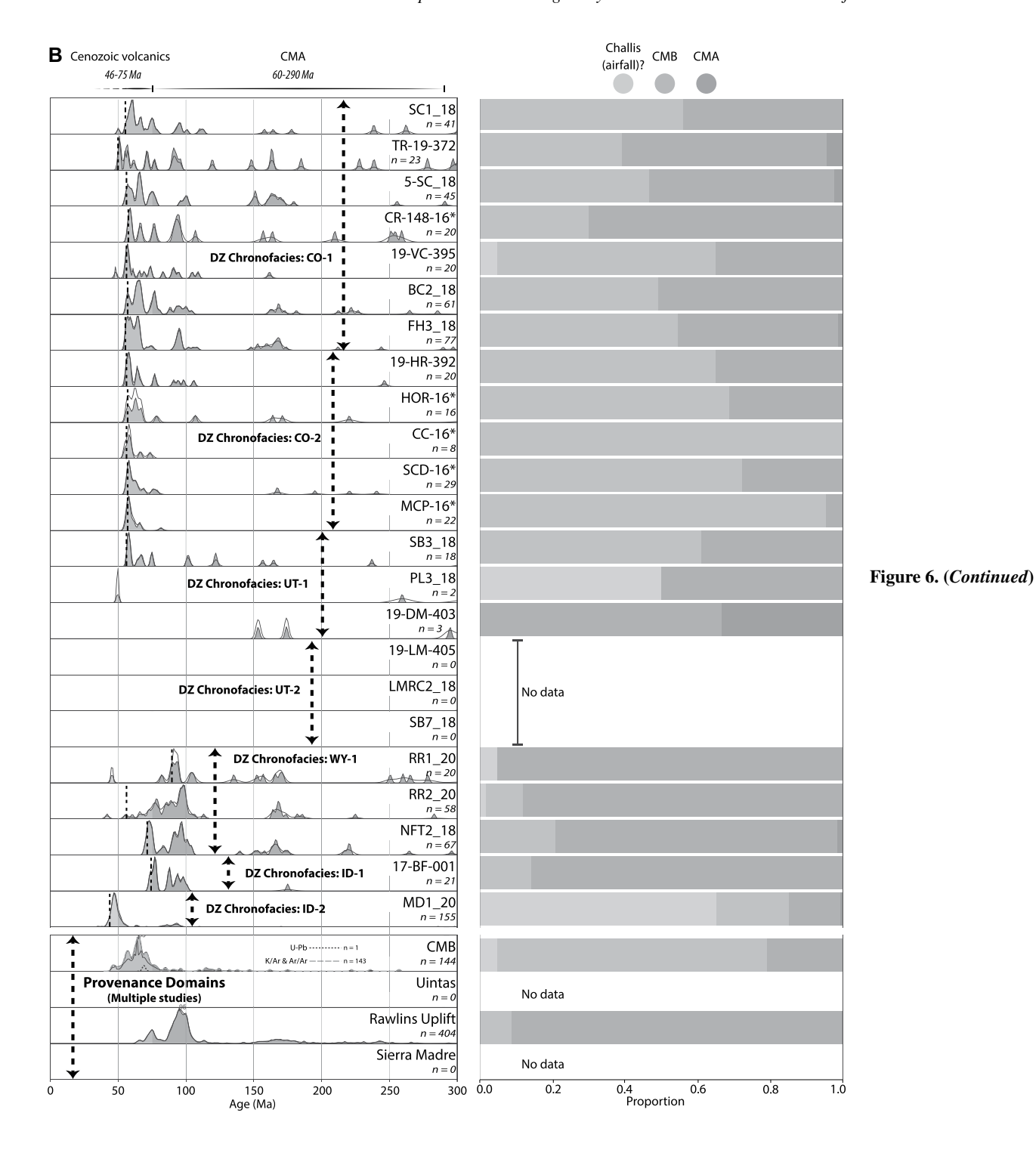
Figure 6. U-Pb detrital zircon kernel density estimate (KDE) spectra for (A) all grains 0-3500 Ma (KDE bandwidth = 15 m.v.) and (B) grains younger than 300 Ma (KDE bandwidth = 1 m.y.(southwestern Wyoming, USA). Detrital zircon (DZ) chronofacies groupings are based on consideration of multi-dimensional scaling analysis and DZmix modeling (Fig. 7). Smaller vertical black dotted lines represent maximum depositional ages (Table 1). n-number of measured grains per sample. Bar plot (right) shows relative proportions of each sample colored by likely original provenance: CMB-Colorado Mineral Belt; CMA-Cordilleran Magmatic Arch; App.-Ouch-Appalachian-Ouachita; Pro.—Grenville Provence; Y-M-Yavapai-Mazatzal; WY **Prov.—Wyoming** province. Provenance age associations are based on prior regional studies by Whitmeyer and Karlstrom (2007); Gehrels et al. (2011); Chapin (2012); Dickinson et al. (2012); Laskowski et al. (2013); and Yonkee et al. (2014) (Fig. 8; Supplemental Text S1 [see text footnote 1]). Provenance source area age spectra are based off previously published geochronologic ages (Premo and Van Schmus, 1989; Souders and Frost, 2006; Dehler et al., 2010; Klein et al., 2010; Lynds and Xie, 2019). Sierra Madre ages represent in situ U-Pb zircon ages compiled from original work by Premo and Van Schmus (1989). Uinta ages represent DZ ages from original work by Dehler et al. (2010).

Colorado Mineral Belt ages represent a compilation of in situ U-Pb, K-Ar, and Ar-Ar ages compiled from the database assembled by Klein et al. (2010). Rawlins Uplift ages represent DZ ages from Lynds and Xie (2019).

zoic populations (Fig. 6). DZ chronofacies ID-1, while similar to WY-1, lacks Mesozoic ages present in WY-1 and shows a far less pronounced Archean Peak. DZ chronofacies ID-2 contains a single, unique Eocene age population. With the exception of one sample (RR1_20, see discussion) MDS analysis clearly

distinguishes distinct Idaho (ID-1 and ID-2) and Wyoming (WY-1) DZ chronofacies from Colorado and Utah DZ chronofacies in both the full age spectrum (Fig. 7A) as well as for ages 0–300 Ma (Fig. 7B). For both age groups DZmix modeling identifies the Rawlins Uplift as the overwhelming source of WY-1 samples,

with minor contributions from the remaining three source domains (Figs. 7 and 8). Obtained petrographic data include an arkosic arenite associated with WY-1 and a subarkose associated with ID-1. MDAs range from 41 Ma to 73 Ma for WY-1, ID-1, and ID-2 (Fig. 6B; Table 1).



DISCUSSION

Detrital Zircon Age Populations

The sandstone samples in this study all represent mixed compositions derived from multiple igneous, sedimentary, and metamorphic sources within the geologically complex central Rocky Mountain region (Fig. 8). Con-

sequently, similar DZ ages may come from more than one source, zircon content may vary between different sources, and some DZ populations may reflect multiple cycles of erosion and deposition. A summary of zircon provenance populations is provided in Table 3 and a more comprehensive discussion is given in the Supplemental Material (Text S1).

Potential Sediment Sources

Three distinct geographic DZ age domains strongly influenced the results: (1) the Sierra Madre Mountains, the Rawlins Uplift, and the Granite Mountains of south-central Wyoming; (2) the Uinta Mountains of southwestern Wyoming and northeastern Utah; and (3) the Park and Sawatch ranges in central Colorado. DZmix pie

TABLE 2. MAXIMUM DEPOSITIONAL AGES VERSUS DATED TUFF AGES (SOUTHWESTERN WYOMING, USA)

Sample name	Stratigraphy	MDA (Ma)	Lower tuff bound	Tuff age (Ma)*	$\pm 2\sigma$	Upper tuff bound	Tuff age (Ma)	\pm 2 σ
17-BF-001	Upper Wasatch Main Body	73.0	N.A.	N.A.	N.A.	Scheggs Bed	52.21	0.09
19-DM-403	WPM: ∼I-bed equivalent	307.5	Layered tuff	50.11	0.09	6th tuff	49.92	0.1
19-HR-392	Upper Cathedral Bluffs	55.8	Layered tuff	50.11	0.09	6th tuff	49.92	0.1
19-LM-405	WPM: ∼I-bed equivalent	931.3	Layered tuff	50.11	0.09	6th tuff	49.92	0.1
19-VC-395	Upper Cathedral Bluffs	55.6	Layered tuff	50.11	0.09	6th tuff	49.92	0.1
5-SC_18	WPM: G-Bed	55.1	Grey tuff	50.86	0.21	Main tuff	50.27	0.09
BC2_18	Upper Cathedral Bluffs	56.0	Layered tuff	50.11	0.09	6th tuff	49.92	0.1
FH3_18	WPM: D-Bed	55.3	Boar tuff	51.13	0.24	Grey tuff	50.86	0.21
LMRC2_18	WPM: ~A-bed equivalent	403.82	Rife tuff	51.61	0.3	Firehole tuff	51.40	0.21
MD1_20	Laney Upper Cathedral Bluffs WPM: ~I-bed equivalent	41.7	6th tuff	49.92	0.1	N.A.	N.A.	N.A.
NFT2_18		69.7	Layered tuff	50.11	0.09	6th tuff	49.92	0.1
PL3_18		330.37	Layered tuff	50.11	0.09	6th tuff	49.92	0.1
RR1_20	Upper Cathedral Bluffs	90.6	Layered tuff	50.11	0.09	6th tuff	49.92	0.1
RR2_20	Laney	56.5	6th tuff	49.92	0.1	N.A.	N.A.	N.A.
SB3_18	WPM: ~I-bed equivalent	57.0	Layered tuff	50.11	0.09	6th tuff	49.92	0.1
SB7_18	WPM: ∼H-bed equivalent	932.59	Layered tuff	50.11	0.09	6th tuff	49.92	0.1
SC1_18	WPM: E-Bed	55.7	Grey tuff	50.86	0.21	Main tuff	50.27	0.09
TR-19-372	WPM: ∼I-bed equivalent	50.6	Layered tuff	50.11	0.09	6th tuff	49.92	0.1

Note: WPM-Wilkins Peak Member; N.A.-not applicable.

*From Smith et al., 2010.

charts visualize relative contributions from each of these source areas to each sample (Fig. 7). Zircon fertility among the domains is likely variable. The Uinta Mountains, in particular, are composed predominately of Grenville-aged sands suggesting higher-than-average zircon fertility (Moecher and Samson, 2006; Dickinson, 2008). Despite this, zircon fertility is a non-issue because all samples were collected from sedimentary strata (fluvial sandstones). Furthermore, the varied, though ubiquitous, presence of Grenville-aged zircons in our data is an archetypal indicator of high fertility (Moecher and Samson, 2006).

The Sierra Madre mountains of south-central Wyoming and northern Colorado are a Laramideaged uplift that exposes the roughly east-towest oriented Cheyenne Belt suture, separating Archean gneisses and metasedimentary sequences to the north from Mesoproterozoic accretionary metamorphic rocks to the south (Karlstrom et al., 1983; Karlstrom and Houston, 1984; Premo and Van Schmus, 1989). Accordingly, the age spectra of zircon derived from this domain are distinctively bimodal, with peaks at ca. 1750 Ma and ca. 2600 Ma (Fig. 6). Based on both petrology and proximity, earlier work on the A-I arkose beds of the Wilkins Peak Member, by Smoot (1983) and Sullivan (1980, 1985) posited the Sierra Madres as the likely source for the arkosic A-I beds from which multiple samples were collected.

To the north of the Sierra Madre, lie the Rawlins Uplift and the Granite Mountains (Fig. 1). The Laramide-aged Rawlins Uplift is an asymmetric, basement-faulted, anticlinal fold that verges to the south (Otteman and Snoke, 2005). The core of the structure is composed of Precambrian basement rock of the Wyoming Province and is flanked to the west by steeply dipping (30°–90°) Cambrian through Late Cretaceous sedimentary cover. Accordingly, DZ spectra associated with the Rawlins Uplift are notably

more complex as they inherit ages from the full Paleozoic-Mesozoic suite flanking the uplifted basement. Age populations for DZ samples associated with the Rawlins Uplift include prominent Cretaceous and Jurassic age populations, as well as a prominent late-Paleoproterozoic peak and a subdued late-Mesoproterozoic population (Lynds and Xie, 2019). For a comprehensive provenance assessment of DZ samples collected adjacent to the Rawlins Uplift, see Lynds and Xie (2019). The Granite Mountains are an east-west trending, Laramide-aged, basement-cored uplift, onlapped to the south by the Eocene Battle Spring Formation, which unconformably overlies the Paleocene Fort Union Formation in the northeast portion of the Great Divide sub-basin. The Battle Spring Formation is an arkosic conglomerate, sandstone, and siltstone deposited in alluvial fans derived from the Granite Mountains (Love, 1970; Pipiringos and Denson, 1970; Lynds and Lichtner, 2016), which is dominated in the south by the Neoarchean Granite Mountains batholith, and in the north hosts granitic and tonalitic gneisses and patches of amphibolite-grade supracrustal rocks >3.2 Ga (Grace et al., 2006).

The Uinta Mountains have been interpreted as a Neoproterozoic north-tilted half-graben that was inverted during the Laramide orogeny (Hansen, 1965; Dehler et al., 2010). Uinta Mountain Group metasedimentary rocks comprise rift fill and have been interpreted to incorporate detritus derived both from the uplifted Grenville-Llano province to the east and from Archean rocks of the Wyoming province to the north. DZ age spectra exhibit major peaks associated with these sources, along with subordinate Mesoproterozoic populations (Fig. 6). Smaller age populations from the early-Mesoproterozoic and Paleoproterozoic, reflecting grains collected along the flow path of the transcontinental fluvial system (Rainbird et al., 2012), are also present.

Central Colorado contains three principal magmatic/metamorphic assemblages: Paleoproterozoic accreted arc terranes, Mesoproterozoic anorogenic granite, and the Colorado Mineral Belt. The latter is a northeast/southwest-trending belt of plutons extending ~500 km, emplaced in three primary stages from ca. 75 Ma to 0 Ma (Fig. 1; Bookstrom, 1990; Chapin et al., 2004; Klein et al., 2010; Chapin, 2012; Gonzales, 2015; Pecha et al., 2018). The oldest and northernmost igneous bodies are primarily alkaline monzonite and quartz monzonite plutons emplaced between 75 Ma and 43 Ma in the northeastern portion of the Colorado Mineral Belt at the eastern edge of the Farallon flat slab. Later episodes of magmatism have been attributed to late Eocene-Oligocene Farallon slab rollback and Rio Grande rifting (Chapin, 2012), but are not relevant to the present study. Magmatic intrusive bodies throughout the Colorado Mineral Belt manifest as stocks, laccoliths, sills, and dikes. Hydrothermal activity associated with Colorado Mineral Belt magmatism resulted in extensive ore deposits (Tweto and Sims, 1963; Bookstrom, 1990). Whole-rock and single mineral measurements of Colorado Mineral Belt plutons suggest that U-Pb data preferentially captures older ages and K-Ar and 40Ar/39Ar data preferentially capture younger ages (Fig. 6; Klein et al., 2010). Speculation as to why this may be is beyond the scope of the current study, but it is clear from the data that igneous bodies associated with the Colorado Mineral Belt were active before and during the deposition of the Green River Formation.

Eocene Watershed Implications

Chronofacies CO-1 and CO-2

DZ chronofacies CO-2 is interpreted to primarily represent sand transported northwestward from central Colorado by the Aspen paleoriver

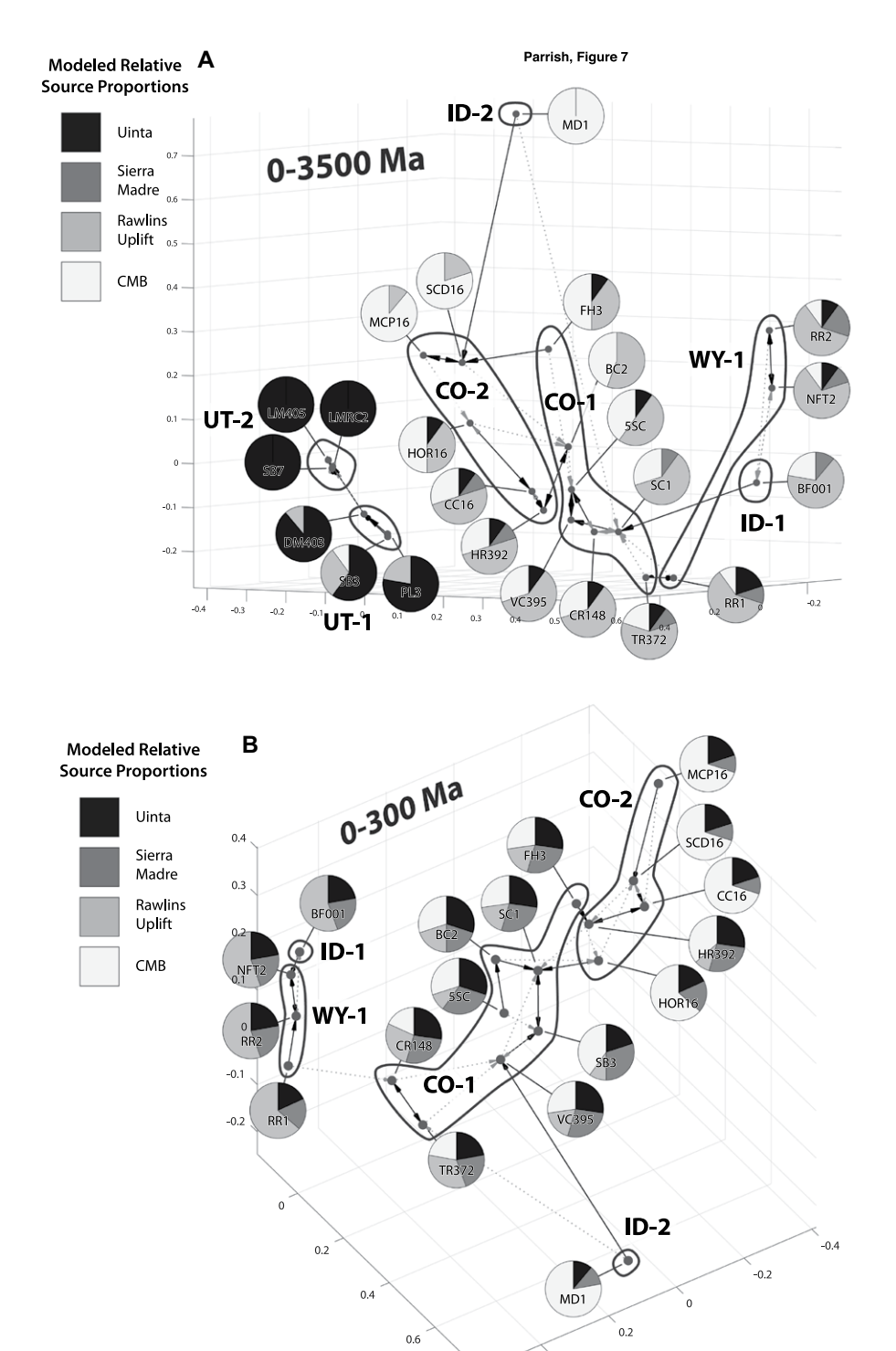


Figure 7. Sample similarity measures, including multi-dimensional scaling (MDS) analysis and DZmix modeling for detrital zircon age populations of (A) 0–3500 Ma and (B) 0–300 Ma (southwestern Wyoming, USA). Distances between samples are plotted on a dimensionless cartesian coordinate grid wherein the distance between similar samples is small relative to the distance between dissimilar samples (Vermeesch, 2013, 2018; Saylor and Sundell, 2016). Each sample is connected to the sample most similar to it by a solid black line capped with a black cone and to the sample second most similar by a dotted gray line capped with a gray cone. Overlain on the MDS plot are DZmix results representing modeled provenance proportions per sample. DZ—detrital zircon; CMB—Colorado Mineral Belt; CMA—Cordilleran Magmatic Arch.

corroborating the work done by Hammond et al. (2019). As the system progressed toward the Bridger sub-basin it was met with contributions from local tributary streams that drained Uinta and Rock Springs uplifts resulting in a dilution of the CO-2 signature and the more complex CO-1 characteristics (Figs. 7 and 9). Alternatively, differences between CO-1 and CO-2 DZ chronofacies may be explainable by sample size. Generally, samples making up DZ chronofacies CO-2 have fewer measured zircons than CO-1; therefore, the complexity seen in CO-1 may be a result of more grains being measured. We believe this is less likely, however, because samples 19-VC-395 and TR-19-372 of CO-1 have similar n-counts to sample 19-HR-392 of CO-2, and sample CR-148-16 of CO-1 has similar n-counts to several samples from CO-2. Higher MDS intersample variation in DZ chronofacies CO-1, CO-2, and WY-1 may be a function of (1) greater grain-age complexity in the Colorado and Wyoming DZ chronofacies relative to the Utah DZ chronofacies and/or in the case of the Colorado DZ chronofacies and (2) the greater number of samples (12) relative to Utah (6).

DZmix identifies the Colorado Mineral Belt and the Rawlins Uplift as the two primary sediment sources of CO-1 and CO-2 DZ chronofacies (Fig. 7). This serves as an important illustration of the limits of DZmix, which cannot resolve differences in provenance when there are similar age ranges from differing source domains. In this case, the DZmix model recognizes the Yavapai-Mazatzal ages present in the Bridger sub-basin as being influenced by the Rawlins Uplift rather than exclusively by the host rocks of the Colorado Mineral Belt. We know this not to be the case, however, due to the lack of Archean ages in CO-1 and CO-2, which would necessarily be present if sediments from the Rawlins Uplift (and thus the Sierra Madre and Granite Mountains) were significantly present in the Bridger sub-basin (discussed below). This illustrates the need for caution when utilizing DZmix to interrogate provenance, and the importance of using multiple means of similarity assessment (in this study DZmix, MDS, and visual spectral analysis) to develop and interpret DZ chronofacies groupings.

Despite its proximity to CO-1 samples in MDS space (Fig. 7A), Sample RR1_20 lacks the diagnostic Paleocene ages indicative of Colorado DZ chronofacies (Fig. 6B) making it more like DZ chronofacies WY-1 (Fig. 7B). The immature, arkosic nature of samples in CO-1 and CO-2 is consistent with first-cycle derivation from crystalline basement and juvenile intrusive or volcanic rocks (Figs. 4 and 5). Further, pervasive seritization of plagioclase feldspar in these samples is indicative of hydrothermal alteration,

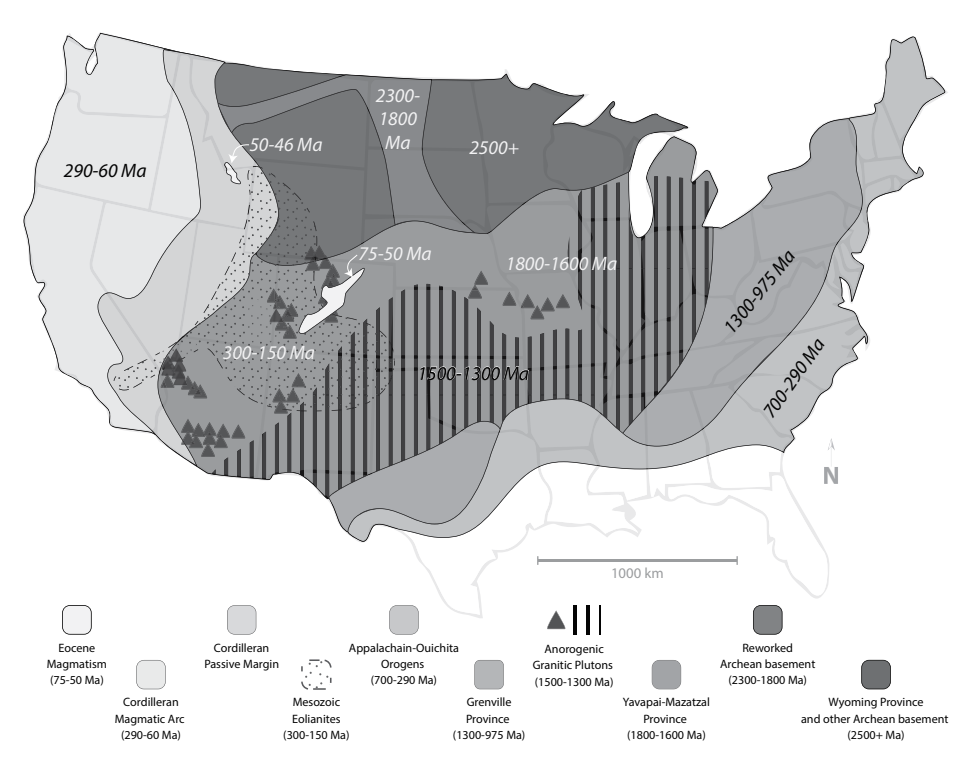


Figure 8. Generalized North American crustal province map (adapted from Gehrels et al., 2011; Laskowski et al., 2013; Pecha et al., 2018). Age domains are shaded to match detrital zircon spectral diagram (Fig. 6). Provenance age associations are based on prior regional studies by Whitmeyer and Karlstrom (2007), Gehrels et al. (2011), Chapin (2012), Dickinson et al. (2012), Laskowski et al. (2013), and Yonkee et al. (2014). Distribution of Mesozoic eolianites from (Leier and Gehrels, 2011).

consistent with derivation from the Colorado Mineral Belt (Fig. 5; Bookstrom, 1990; Nesse, 2012). Paleocurrent data from Hammond et al. (2019) and Forss (1983) support the existence of a northwest-flowing Aspen paleoriver (Fig. 3), but CO-1 paleocurrent data collected for this study are more ambiguous (e.g., sample BC2_18, Fig. 3). This ambiguity may in part reflect the generally finer-grained nature of the fluvial sandstone facies examined in this study, which contain fewer reliable paleocurrent indicators. Alternatively, the depositional nature of the paleoriver system remains in question and paleo-

TABLE 3. NORTH AMERICAN DETRITAL ZIRCON PROVENANCE AGES

ZITIOONT	HOVENANOE AGES
DZ age population (Ma)	Most likely source(s)
3500–2500	Basement-cored, Laramide structures
2300–1800	Trans-Hudson Province, Snowy Pass Supergroup
1800–1600	Snowy Pass Supergroup Yavapai and Mazatzal provinces
1480-1340	A-type igneous plutons
1200-975	Grenville-Llano province
290–75	Cordilleran Magmatic Arc
75–50	Colorado Mineral Belt

Note: See Supplemental Text S1 (see text footnote 1) for details. DZ—detrital zircon.

current indicators at Badger Creek and Scrivener Butte may record meanders or other local departures from the primary river trajectory.

Chronofacies UT-1 and UT-2

Both UT-1 and UT-2 are interpreted as representing sediment shed proximally off the Uinta Mountains. Minimal MDS inter-sample variation in DZ chronofacies UT-1 and UT-2 suggests less age complexity in the source domains and/or less potential for inherited complexity between source and sink, and northward paleocurrent indicators are consistent with a more proximal source (Figs. 3 and 5). UT-2 framework grain compositions are dominantly quartzose, consistent with greater mineralogic maturity caused by multiple cycles of erosion and transport while UT-1 framework grain compositions are more variable (Fig. 4). Dehler et al. (2010) proposed that a major paleoriver system carried sediment derived from the Grenville orogen and its foreland westward across the continent to the Uinta graben, depositing Neoproterozoic Uinta Mountain Group strata that locally reach \sim 7 km in thickness. Subsequent Paleozoic sedimentary strata covered the Uinta Mountain Group before diachronous uplift and unroofing from

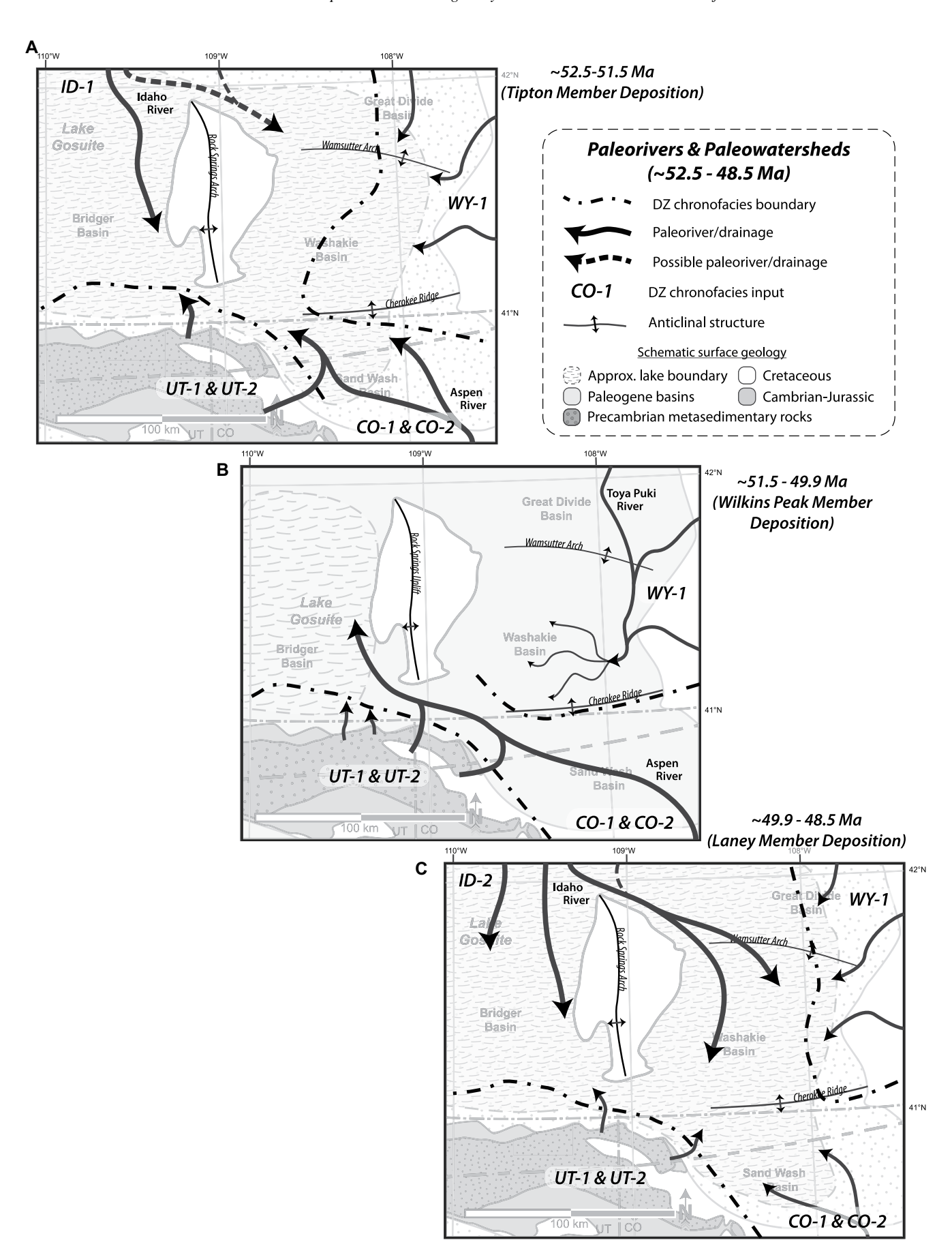
the Paleogene through the early Eocene (Smith et al., 2015). Differences in UT-1 and UT-2, however, are inexplicable by unroofing patterns since we would expect to see (1) the Paleozoic ages associated with UT-1 to be both closer to the uplift and farther east than they are, neither of which is true, and (2) stratigraphic organization of the two DZ chronofacies, which is similarly not present. UT-1 and UT-2 are therefore interpreted to be primarily from the recycling of sedimentary and metasedimentary strata within and adjacent to the Uinta Uplift, and UT-1's Paleozoic populations are interpreted to be recycled from late Paleozoic and Mesozoic strata, specifically the Triassic-Jurassic aeolian sedimentary units recycling out of the fold-thrust belt to the west (Figs. 6A and 7; Leier and Gehrels, 2011; Lawton et al., 2010). Sample SB3_18's notable Paleocene age population is discussed below.

Also of note is the lack of Neoarchean ages in either UT-1 or UT-2 relative to the compiled source spectra (Fig. 6A). In a study by Dehler et al. (2010), Neoarchean zircon grains are prominent in most samples and were attributed to local derivation from the southern Wyoming Province. They vary in abundance in Neoproterozoic units of the western Uinta Mountains from dominant to nearly absent (Yonkee et al., 2014). The lack of Neoarchean grains in our samples likely reflects their local absence in parent Neoproterozoic source rocks. Alternatively, Grenville-age zircons in UT-1 and UT-2 could also be derived from Mesozoic aeolian sandstone units that flank the northern Uinta Uplift. Colorado Plateau aeolianites to the south contain abundant Grenville-age zircons (Dickinson and Gehrels, 2003, 2009a). Mesozoic aeolianites typically also contain major Appalachian-derived post-Grenville zircon populations, however, which are present in only minor quantities in UT-1 and absent altogether in UT-2 (Fig. 6A).

Chronofacies WY-1, ID-1, and ID-2

WY-1 samples are interpreted as representing influence from uplifts to the east and north of the Greater Green River Basin. While DZmix identifies Colorado Mineral Belt and Uinta sources in WY-1 samples (Fig. 7), based on the

Figure 9. Paleowatershed reconstructions for the (A) Tipton Member, (B) Wilkins Peak Member, and (C) Laney Member deposition, as well as age-equivalent strata of the Green River Formation of the western USA. Known paleoriver systems include the Aspen, Idaho, and Toya Puki. Possible paleodrainage pathways, recognized detrital zircon (DZ) chronofacies boundaries and inputs, and pertinent structural features are also shown. Approx.—approximate.



geographic distribution of these samples, we believe that neither the Uinta Mountains nor the Colorado Mineral Belt has any influence on WY-1 samples and that all ages present can be attributed to either basement or cover strata associated with the Rawlins, Sierra Madre, and Granite uplifts. We propose the existence of an early Eocene paleoriver, herein named "Toya Puki" River, meaning "Mountain Fan," honoring the Eastern Shoshone and their ancestral land. The Toya Puki paleoriver flowed south from the Granite Mountains and Rawlins uplifts picking up drainage from the Sierra Madre prior to terminating in the Washakie sub-basin. The prominent Archean and late-Paleoproterozoic peaks in WY-1 suggest significant influence from the Sierra Madre Uplift as they provide the closest primary source for both age groups (Lynds and Xie, 2019). Recycling from cover strata associated with these uplifts also accounts for subdued Paleozoic and Mesoproterozoic age populations most likely inherited from North American passive margin strata, Paleozoic sandstones in surrounding areas, and/or Mesozoic eolianites. In the absence of influence from the Colorado Mineral Belt, which is supported by the lack of Paleocene ages as well as paleocurrent indicators (Figs. 3 and 6B), the Late Cretaceous ages present in WY-1 are likely indicative of recycled grains originating in the Cordilleran magmatic arc then transported east as part of a Cretaceous dispersal system.

As the only sample making up DZ chronofacies ID-2, sample MD1_20 has a single distinct Eocene peak at ca. 47 Ma. At this time the Greater Green River Basin was filling with volcaniclastic sediment largely derived from the Challis Volcanic field (49.8–45.5 Ma) sourced more than 400 km northwest by the Idaho paleoriver (Chetel et al., 2011; Honig et al., 2020). As such, MD1_20, which was collected stratigraphically above the Cathedral Bluffs Member, represents the exclusive influence of the Idaho Paleoriver as it filled the Greater Green River Basin from the north.

We differentiate between DZ chronofacies ID-1 (comprised solely of sample 17-BF-001) and DZ chronofacies WY-1 based on the differences in Mesozoic and Archean ages and attribute these variations to stratigraphic and geographic differences between 17-BF-001 and the other three samples. Where samples NFT2_18, RR2_20, and RR1_20 were all collected near the contact between the Cathedral Bluffs and Laney members in the Washakie sub-basin, 17-BF-001 was collected near the top of the Wasatch Main Body member in the Bridger sub-basin, making it ∼5 m.y. older (Figs. 1B and 2; Smith et al., 2008). Sample 17-BF-001 contains zircons sourced from the north by the Idaho paleoriver.

This interpretation is in line with interpretations made by Honig et al. (2020) and DZ ages for sample 17-BF-001 closely resemble samples collected from the Wasatch Main Body associated with the Idaho paleoriver farther north.

The presence of sample 17-BF-001 additionally suggests a shift in fluvial input to the Bridger sub-basin. Prior to ca. 53 Ma, Idaho paleoriver-derived zircon grains are prominent, whereas these grains are absent during the deposition of the Wilkins Peak Member. As evidenced by DZ chronofacies CO-1 and CO-2, however, fluvial input to the same area was dominantly from the southeast during Wilkins Peak Member deposition. Influence from the Idaho paleoriver seems to return and dominate again after Wilkins Peak/Cathedral Bluffs Member deposition as suggested by the presence of DZ chronofacies ID-2 (sample MD1_20).

Lateral DZ Chronofacies Transitions

Age-equivalent strata record profound differences in provenance over short distances. Based on field relationships to each other and to lacustrine facies that contain dated tephras, samples in DZ chronofacies CO-1, CO-2, UT-1, and UT-2 (with the exception of CR-148-16) were all deposited synchronously or nearly so (c.f., Smith et al., 2008, 2015). Lateral transitions between these DZ chronofacies, therefore, are interpreted to reflect contemporaneous depositional systems that competed to fill available basin accommodation, rather than secular changes in sources over time. The spatial stability of these deposystems is supported by the consistency of zircon ages in samples taken from different stratigraphic levels in the same general area. For example, samples SC1_18, FH3_18, and 5-SC_18 are all part of DZ chronofacies CO-1 and collected from the Bridger sub-basin near its evaporite depocenter. Meanwhile, samples LMRC2_18, 19-LM-405, 19-DM-403, and PL3_18 are all either DZ chronofacies UT-1 or UT-2 and were collected at the southern margin of the Bridger sub-basin near the Uinta Uplift (Figs. 1-3). This suggests that the lateral transitions in sandstone provenance may occur on a kilometer scale. Samples FH3_18, SC1_18, and 5-SC_18 were collected only ~25 km north of samples LMRC2_18, 19-LM-405, 19-DM-403, and PL3_18, yet they represent sand sources originating hundreds of kilometers apart. Moreover, samples SB3_18 and SB7_18 were collected ~5 km apart in what appears to be the same outcropping sandstone interval and show similar paleocurrent flow directions. Despite this, SB3_18 and SB7_18 display clear differences in petrography and DZ ages. Deposits at such localities, due to the dynamic and avulsive nature of distributive river systems (Mohrig et al., 2000; Weissmann et al., 2010, 2015; Best and Fielding, 2019) record reworked sediments from both sources, yet the abruptness (<5 km) of the mixing line between the Aspen paleoriver and tributaries that drained the Uinta Uplift (Fig. 9B) suggests relatively discrete and consistent depositional features during the deposition of the Wilkins Peak Member.

DZ chronofacies boundaries may also reflect the interaction of depositional systems with intrabasinal structural relief. Despite close proximity (<20 km) to the Aspen paleoriver system, mixing of the Toya Puki paleoriver system with the Aspen paleoriver appears limited based on the notable dearth of Archean-aged grains associated with DZ chronofacies CO-1 and CO-2 (Fig. 6A). The Toya Puki paleoriver system appears to have terminated within the Washakie sub-basin. One possibility is that the Washakie sub-basin may have contained a lake that captured the Toya Puki paleoriver thus precluding it from joining the Aspen paleoriver. Alternatively, the Washakie basin may have been "hemiendorheic" (Por, 2000) impounded to the south by the Cherokee Ridge and to the west by the Rock Springs Uplift (Fig. 9B). As such the Toya Puki paleoriver may have succumbed to evaporation rather than joining the Aspen paleoriver as a tributary. Modern analogs for this type of system include the Pantanal region as fed by the Taquari River in central South America and the Okavango Delta fed by the Cubango River in south-central Africa. In either case, precedent for Greater Green River sub-basin accommodation is seen north in the Great Divide sub-basin, wherein the Battle Spring Formation represents continual fill of the basin beginning in the earliest Eocene and extending to the early middle Eocene-a timespan equal to that of the deposition of the Wasatch and Green River formations combined (Pipiringos and Denson, 1970).

The presence of Aspen paleoriver-derived ages (Sample BC2_18) north of Cherokee Ridge and on the western edge of the Washakie subbasin, however, suggests that either the Aspen paleoriver produced enough sediment to periodically overcome Cherokee Ridge from south to north, or that it circumnavigated the structure to the west thus adding to the infill of Washakie sub-basin en route to the Bridger sub-basin. In either case, any mixing between the Aspen and Toya Puki paleoriver systems occurred in the Washakie sub-basin, which provided the terminal sink for the Toya Puki paleoriver at the time.

Based on the presence of DZ chronofacies WY-1 in the Washakie sub-basin, the Washakie and Great Arch, which separates the Washakie and Great Divide sub-basins, lacked surface expression and was not a barrier to the Toya Puki paleoriver

entering the Washakie sub-basin. Alternatively, the Toya Puki paleoriver may have circumnavigated the structural high to the east during the deposition of the Cathedral Bluffs Member, but the arch was certainly overcome by the Idaho paleoriver during the deposition of the Laney Member, as evidenced by sample MD1_20 and DZ chronofacies ID-2 (Figs. 6 and 9C).

Regional Implications

In considering Laramide foreland basins, it is often assumed that sediments are sourced proximally (e.g., Dickinson et al., 1988). Though relatively limited, more recent assessments of the relationships of Laramide foreland paleo-watersheds to paleo-lakes reveal that a substantial portion of the water entering a lake may have been transported long distances (e.g., 100-1000 km) by rivers (e.g., Davis et al., 2010; Dickinson et al., 2012; Hammond et al., 2019), and may have originated at relatively high elevations (e.g., Dettman and Lohmann, 2000; Carroll et al., 2008; Fan and Dettman, 2009; Chetel et al., 2011; Fan et al., 2014; Schneider et al., 2016; Ma et al., 2017). This study supports these previous findings as it recognizes sediments sourced from four distinct watersheds as proximally as the Uinta (<30 km) and Sierra Madre mountains (<50 km) and as distally as the Granite Mountains (>120 km), the Colorado Mineral Belt (>300 km), and central Idaho (>400 km) to the Greater Green River Basin. Moreover, this study offers context on the timing of uplift and accommodation generation for intrabasinal Greater Green River Basin Laramide structures. Based on our findings, and findings by Hammond et al. (2019), drainage organizations within the surrounding region (and changes therein) may be equally as important as local climate change in controlling the overall character of lake deposits.

It is well-established that during the Late Cretaceous, sediment dispersal throughout what is now the intermountain west was dominantly eastward, driven by the Sevier thrust front (e.g., DeCelles, 2004). How and when this system was dissected and reoriented during the Paleocene and Eocene remains a topic of interest. Due to the temporal scope of our data, comment on the onset of Laramide Uplift is beyond the purview of this paper. However, the ubiquitous presence of pre-Cambrian ages across our samples corroborates that extrabasinal Laramide structures including the Sierra Madre Mountains, the Rawlins Uplift and the Granite Mountains of south-central Wyoming, the Uinta Mountains of southwestern Wyoming and northeastern Utah, and the Park and Sawatch ranges in central Colorado were all established sediment sources by the early-Eocene (e.g., Bookstrom, 1990; Carroll et al., 2006; Lynds and Xie, 2019). Lynds and Xie (2019) posit the dominance of an east-ward propagating sediment system throughout the Bridger sub-basin and into the Hanna Basin as late as the Paleocene Fort Union Formation. Our data suggest that immediately thereafter, long-distance (>100 km), west- and southwest-ward-flowing paleorivers including the Aspen and Toya Puki paleorivers were established as sediment dispersal systems into the western and southern Greater Green River Basin.

Hammond et al. (2019) posited that the influence of the Aspen paleoriver provided the requisite alkalinity for the formation of trona-a Nacarbonate evaporite—in the Bridger sub-basin. The highest frequency of bedded evaporites in the Bridger sub-basin occurs stratigraphically below sample FH3_18 (Fig. 2B; Pietras and Carroll, 2006; Smith et al., 2014), implying that the Aspen paleoriver influenced Lake Gosiute and the Bridger sub-basin as far back as the start of the Wilkins Peak Member. The presence of sample CR-148-16 (DZ chronofacies CO-1) in the Sand Wash sub-basin, however, suggests that the Aspen paleoriver influenced the Sand Wash sub-basin prior to the Wilkins Peak Member during the deposition of the Main Body of the early-Eocene Wasatch Formation. This establishes westward long-distance drainage, opposite that of the long-standing Cretaceous-Paleocene trend, by the earliest Eocene.

Differences between coeval samples 17-BF-001 and CR-148-16 (notably Paleocene, mid-Mesoproterozoic, and Archean DZ age populations) suggest that the Aspen Paleoriver did not make its way into the Bridger sub-basin until Wilkins Peak Member times and that until then, the Bridger sub-basin was largely influenced by fluvial input from the north (see discussion on Idaho DZ chronofacies; Fig. 9). Regardless, by the early Eocene, influence of the Uintas in the Sand Wash sub-basin is negligible. Potential reasons for this include decreasing accommodation in the basin as the depocenter shifted west toward the Bridger sub-basin (possibly due to increased input from the Colorado Mineral Belt), diachronous uplift of the Uintas that shifted sedimentation westward (e.g., Smith et al., 2015), denudation of the Uintas resulting in less distal deposition, or some combination thereof. Input from the Uintas (UT-1 and UT-2) was likely consistent throughout the Wilkins Peak Member. Uplift of the Uinta Mountains occurred as part of the greater Laramide deformation, thus largely predating the Eocene Wilkins Peak Member (Bruhn et al., 1989; Smith et al., 2015). In the Uinta Basin, fluvial sediments sourced from the Uinta Uplift are recognized as early as the Maastrichtian, suggesting that sediment delivery from the Uintas was likely ongoing throughout the deposition of the Wasatch Formation as well (Picard et al., 1983; Bruhn et al., 1989; Roehler, 1992; Carroll et al., 2006; Smith et al., 2015). Despite this, UT-1 and UT-2 terminate $<\sim$ 30 km from the estimated watershed boundary. Comparatively, in the Uinta Basin to the south, Eocene fluvial deposits associated with the Uinta Mountains have been recognized >45 km from the estimated watershed boundary (Fouch, 1981; Picard et al., 1983). This suggests limited catchment for, or supply of, sediment issuing north off the Uintas into the Bridger sub-basin. Structurally, the Uinta Mountains are a north-verging anticlinal feature (Bruhn et al., 1983). As a result, the northern watershed, supplying sediment to the Bridger sub-basin, appears to have been smaller than the southern watershed, which terminates into the Uinta Basin, resulting in greater sedimentation to the Uinta Basin than the Bridger (Allen et al., 2013).

Intrabasinal structures including the Cherokee Ridge and the Rock Springs Uplift were present and topographically exposed by Wilkins Peak Member time as evidenced by the isolation of the Toya Puki Paleoriver from the Aspen Paleoriver (Fig. 9B). If the Wamsutter Arch was present then, it is unlikely that it created any relief given the transport of sediment south from the Granite Mountains and Rawlins Uplift by the Toya Puki River during the early Eocene (Fig. 9).

Post-Wilkins Peak Member deposition of the Laney Member is characterized by freshwater and "over-filled" lake-type facies (Carroll and Bohacs, 1999; Rhodes and Carroll, 2015). This shift has been attributed to the recapture of the Idaho paleoriver (Fig. 9C; Chetel et al., 2011; Honig et al., 2020), which is supported by our data, as well as watershed expansion (Rhodes and Carroll, 2015). Throughout the deposition of the Laney Member, both paleoriver systems simultaneously filled the Greater Green River Basin, but the relative contribution of the Idaho paleoriver system was greater, as volcaniclastics brought by the Idaho paleoriver ultimately filled the Greater Green River Basin by the end of Laney Member deposition (Fig. 9C; Roehler, 1992; Carroll and Bohacs, 1999). Further work is needed to understand the evolution and influence of the Idaho paleoriver through Green River Formation time.

CONCLUSIONS

Using DZ analysis on fluvial samples collected in three of the Greater Green River subbasins, we were able to identify seven distinct DZ chronofacies associated with four separate source regions and watersheds in the southern and eastern reaches of the Greater Green River Basin. These DZ chronofacies are further cor-

roborated by petrographic, paleocurrent, and MDA data. DZ chronofacies CO-2 primarily represents sand transported northwestward from central Colorado by the Aspen paleoriver, corroborating previous work done by Hammond et al. (2019) (Figs. 6 and 9). As the system progressed toward the Bridger sub-basin it was met with contributions from local tributary streams that drained the Uinta Uplift resulting in the more complex characteristics of DZ chronofacies CO-1 down system (Figs. 6, 7, and 9). DZ chronofacies UT-1 and UT-2 are associated with tributaries issuing out of the Uinta Uplift and are comprised of sediment primarily recycled out of sedimentary and metasedimentary strata within and adjacent to the uplift (Figs. 6 and 9). DZ chronofacies WY-1 is indicative of primary and recycled sediments associated with the Toya Puki paleoriver and weathering out of the Sierra Madre, Rawlins, and Granite uplifts of south and central Wyoming. Contrary to previous suppositions, sediment from the Toya Puki paleoriver does not join the Aspen paleoriver headed to the Bridger sub-basin but is instead sequestered in the Washakie sub-basin, likely baffled by the Cherokee Ridge to the south (Figs. 6 and 9). DZ chronofacies ID-1 and ID-2 represent sedimentation via the Idaho paleoriver before and after Wilkins Peak Member deposition, respectively, implying that the Idaho paleoriver was not a contributing source to the Greater Green River Basin through Wilkins Peak Member deposition (e.g., Chetel et al., 2011; Honig et al., 2020).

The results of this study reveal a surprising complexity of sandstone provenance within a relatively small area, reflecting sand derived from diverse local and distal sources. Moreover, lateral transitions between different DZ chronofacies can occur over distances as little as 5 km, implying that different depositional features maintained discrete positions within the basin over millions of years rather than avulsing across it. Recognition of these complexities was made possible by high sample density, contrasting with regional- to continental-scale provenance studies with sampling densities that are often an order of magnitude lower (e.g., Laskowski et al., 2013; Gehrels and Pecha, 2014; Blum et al., 2017). These two approaches complement one another, with large-scale studies providing needed tectononomagnetic context and smallscale studies offering a clearer view of local sediment dispersal.

Finally, the complexity of these systems indicates a need for caution in conducting thermochronology or paleoaltimetry studies. The latter often use early, authigenic carbonate phases in basinal fluvial and floodplain deposits to infer precipitation δ^{18} O associated with upstream mountain ranges (e.g., Chamberlain and Poage,

2000; Chamberlain et al., 2012; Gao and Fan, 2018). The results of this study demonstrate that the deposits of rivers originating hundreds of kilometers away may reside closely adjacent to detritus derived from local uplifts. Detailed provenance studies are therefore critical to avoid misinterpretation of the drainage pathways that linked high-elevation sediment sources to low-elevation deposits.

ACKNOWLEDGMENTS

We are grateful to T. Lawton, S.R. Meyers, S.P. Peters, and B. Tikoff for their helpful comments, conversations, and insights throughout the research and writing of this paper. This paper significantly benefitted from reviews by anonymous reviewers, whom we thank for their thoughtful and insightful comments. We are additionally grateful to the Arizona Laserchron Center (Tucson, Arizona, USA), specifically, Daniel Alberts and Mark Pecha for their correspondence and support before, during, and after the use of the facilities. This study would not have been possible without the use of Brad Singer's WiscAr Geochronology Laboratory and specifically the help of Bryan Wathen in the zircon separation process and Bil Schneider for imaging assistance. We are especially grateful to Robyn Rofkar and the Eastern Shoshone Cultural Center (Fort Washakie, Wyoming, USA) for advice and assistance in naming the hypothesized Toya Puki paleoriver and to C. Kortyna for technical detrital zircon advice. Funding for this research was provided by the National Science Foundation Division of Earth Sciences 1813278, the American Association of Petroleum Geologists Robert and Carolyn Maby Memorial Grant, the Rocky Mountain Section Society for Sedimentary Geology (SEPM) 2018 Fluvial Sedimentology Award, a SEPM Student Research Grant, and the Department of Geoscience, University of Wisconsin-Madison (Madison, Wisconsin, USA).

REFERENCES CITED

- Allen, P.A., and Allen, J.R., 2013, Basin Analysis: Principles and Application to Petroleum Play Assessment: Hoboken, New Jersey, John Wiley & Sons, v. 53, p. 1689– 1699.
- Allen, P.A., Armitage, J.J., Carter, A., Duller, R.A., Michael, N.A., Sinclair, H.D., Whitchurch, A.L., and Whittaker, A.C., 2013, The Qs problem: Sediment volumetric balance of proximal foreland basin systems: Sedimentology, v. 60, p. 102–130, https://doi.org/10.1111/sed .12015.
- Aswasereelert, W., Meyers, S.R., Carroll, A.R., Peters, S.E., Smith, M.E., and Feigl, K.L., 2013, Basin-scale cyclostratigraphy of the Green River Formation, Wyoming: Geological Society of America Bulletin, v. 125, p. 216–228 https://doi.org/10.1130/B30541.1.
- Ball, T.T., and Farmer, G.L., 1998, Infilling history of a Neoproterozoic intracratonic basin: Nd isotope provenance studies of the Uinta Mountain Group, Western United States: Precambrian Research, v. 87, p. 1–18 https://doi .org/10.1016/S0301-9268(97)00051-X.
- Best, J.I.M., and Fielding, C.R., 2019, Describing fluvial systems: Linking processes to deposits and stratigraphy, in Corbett, P.W.M., Owen, A., Hartley, A.J., Pla-Pueys, S., Barreto, D., Hacknet, C., and Kape, S.J., eds., River to Reservoir: Geoscience to Engineering: Geological Society, London, Special Publication 488, p. 152–166, https://doi.org/10.1144/SP488-2019-056.
- Bird, P., 1984, Laramide crustal thickening event in the Rocky Mountain Foreland and Great Plains: Tectonics, v. 3, p. 741–758, https://doi.org/10.1029 /TC003i007p00741.

- Bird, P., 1998, Kinematic history of the Laramide orogeny in latitudes 35°–49°N, western United States: Tectonics, v. 17, p. 780–801, https://doi.org/10.1029/98TC02698.
- Blum, M.D., Milliken, K.T., Pecha, M.A., Snedden, J.W., Frederick, B.C., and Galloway, W.E., 2017, Detritalzircon records of Cenomanian, Paleocene, and Oligocene Gulf of Mexico drainage integration and sediment routing: Implications for scales of basin-floor fans: Geosphere, v. 13, p. 2169–2205 https://doi.org/10.1130 /GES01410.1.
- Bookstrom, A.A., 1989, The Climax-Alma granite batholith of Oligocene age and the porphyry molybdenum deposits of Climax, Colorado, U.S.A: Engineering Geology, v. 27, p. 543–568 https://doi.org/10.1016 //0013-7952(89)90045-8.
- Bookstrom, A.A., 1990, Igneous rocks and carbonate-hosted ore deposits of the Central Colorado Mineral Belt, in Beaty, D.W., Landis, G.P., and Thompson, T.B., eds., Carbonate-Hosted Sulfide Deposits of the Central Colorado Mineral Belt: Society of Economic Geologists, Economic Geology Monograph Series 7, p. 45–65.
- Bradley, W.H., 1964, Geology of Green River Formation and Associated Eocene Rocks in Southwestern Wyoming and Adjacent Parts of Colorado and Utah: U.S. Geological Survey Professional Paper 496-A, 90 p., https:// pubs.er.usgs.gov/publication/pp496A.
- Brown, E.T., Stallard, R.F., Larsen, M.C., Bourlès, D.L., Raisbeck, G.M., and Yiou, F., 1998, Determination of predevelopment denudation rates of an agricultural watershed (Cayaguás River, Puerto Rico) using in-situproduced 10Be in river-borne quartz: Earth and Planetary Science Letters, v. 160, p. 723–728 https://doi.org /10.1016/S0012-821X(98)00123-X.
- Bruck, B.T., Schmitz, M.D., Carroll, A.R., Meyers, A.R., Walters, A.P., and Jicha, B., 2023, Astronomical and tectonic influences on climate and deposition revealed through radioisotopic geochronology and Bayesian age-depth modeling of the Early Eocene Green River Formation, Wyoming: Geological Society of America Bulletin (in press), https://doi.org/10.1130/B36584.1.
- Bruhn, R.L., Picard, M.D., and Beck, S.L., 1983, Mesozoic and early Tertiary paleostructure and sedimentology of central Wasatch Mountains, Uinta Mountains, and Uinta Basin: AAPG Bulletin, v. 67, p. 63–105, https://doi.org /10.1306/03b5b95c-16d1-11d7-8645000102c1865d.
- Bruhn, R.L., Picard, M.D., and Isby, J.S., 1989, Tectonics and sedimentology of Uinta Arch, Western Uinta Mountains, and Uinta Basin, in Peterson, J.A., ed., Paleotectonics and Sedimentation in the Rocky Mountain Region, United States: AAPG Memoir 41, p. 333–352, https://doi.org/10.1306/M41456C16.
- Capaldi, T.N., Horton, B.K., McKenzie, N.R., Stockli, D.F., and Odlum, M.L., 2017, Sediment provenance in contractional orogens: The detrital zircon record from modern rivers in the Andean fold-thrust belt and foreland basin of western Argentina: Earth and Planetary Science Letters, v. 479, p. 83–97 https://doi.org/10.1016 /j.epsl.2017.09.001.
- Carroll, A.R., and Bohacs, K.M., 1999, Stratigraphic classification of ancient lakes: Balancing tectonic and climatic controls: Geology, v. 27, p. 99–102 https://doi.org/10.1130/0091-7613(1999)027<0099:SCOALB>2.3.CO;2.
- Carroll, A.R., Chetel, L.M., and Smith, M.E., 2006, Feast to famine: Sediment supply control on Laramide basin fill: Geology, v. 34, p. 197–200 https://doi.org/10.1130 /G22148.1.
- Carroll, A.R., Doebbert, A.C., Booth, A.L., Chamberlain, C.P., Rhodes-Carson, M.K., Smith, M.E., Johnson, C.M., and Beard, B.L., 2008, Capture of high-altitude precipitation by a low-altitude Eocene lake, western U.S: Geology, v. 36, p. 791–794, https://doi.org/10 .1130/G24783A.1.
- Chamberlain, C.P., and Poage, M.A., 2000, Reconstructing the paleotopography of mountain belts from the isotopic composition of authigenic minerals: Geology, v. 28, p. 115–118 https://doi.org/10.1130/0091-7613(2000)28<115:RTPOMB>2.0.CO;2.
- Chamberlain, C.P., Mix, H.T., Mulch, A., Hren, M.T., Kent-Corson, M.L., Davis, S.J., Horton, T.W., and Graham, S.A., 2012, The Cenozoic climatic and topographic evolution of the western North American Cordil-

- lera: American Journal of Science, v. 312, p. 213–262 https://doi.org/10.2475/02.2012.05.
- Chapin, C.E., 2012, Origin of the Colorado Mineral Belt: Geosphere, v. 8, p. 28–43 https://doi.org/10.1130 /GES00694.1.
- Chapin, C.E., Wilks, M., and Mcintosh, W.C., 2004, Spacetime patterns of Late Cretaceous to present magmatism in New Mexico: Comparison with Andean volcanism and potential for future volcanism: New Mexico Bureau of Geology and Mineral Resources Bulletin, p. 13–40.
- Chetel, L.M., Janecke, S.U., Carroll, A.R., Beard, B.L., Johnson, C.M., and Singer, B.S., 2011, Paleogeographic reconstruction of the Eocene Idaho River, North American Cordillera: Geological Society of America Bulletin, v. 123, p. 71–88 https://doi.org/10.1130/B30213.1.
- Culbertson, W.C., 1961, Stratigraphy of the Wilkins Peak Member of the Green River Formation: Firehole Basin Quadrangle, Wyoming: U.S. Geological Survey Professional Paper 424-D, p. 170–173.
- Davis, S.J., Dickinson, W.R., Gehrels, G.E., Spencer, J.E., Lawton, T.F., and Carroll, A.R., 2010, The Paleogene California River: Evidence of Mojave-Uinta paleodrainage from U-Pb ages of detrital zircons: Geology, v. 38, p. 931–934, https://doi.org/10.1130/G31250.1.
- DeCelles, P.G., 2004, Late Jurassic to Eocene evolution of the Cordilleran thrust belt and foreland basin system, western U.S: American Journal of Science, v. 304, p. 105–168, https://doi.org/10.2475/ajs.304.2.105.
- Dehler, C.M., Fanning, C.M., Link, P.K., Kingsbury, E.M., and Rybczynski, D., 2010, Maximum depositional age and provenance of the Uinta Mountain group and big cottonwood formation, northern Utah: Paleogeography of rifting western Laurentia: Geological Society of America Bulletin, v. 122, p. 1686–1699, https://doi.org /10.1130/B30094.1.
- Delaney, I., Bauder, A., Huss, M., and Weidmann, Y., 2018, Proglacial erosion rates and processes in a glacierized catchment in the Swiss Alps: Earth Surface Processes and Landforms, v. 43, p. 765–778 https://doi.org/10 .1002/esp.4239.
- Dettman, D.L., and Lohmann, K.C., 2000, Oxygen isotope evidence for high-altitude snow in the Laramide Rocky Mountains of North America during the Late Cretaceous and Paleogene: Geology, v. 28, p. 243–246, https://doi.org/10.1130/0091-7613(2000)28<243:OIEFHS>2 .0.CO;2.
- Dickinson, W.R., 2008, Impact of differential zircon fertility of granitoid basement rocks in North America on age populations of detrital zircons and implications for granite petrogenesis: Earth and Planetary Science Letters, v. 275, p. 80–92 https://doi.org/10.1016/j.epsl.2008.08.003.
- Dickinson, W.R., and Gehrels, G.E., 2003, U-Pb ages of detrital zircons from Permian and Jurassic eolian sandstones of the Colorado Plateau, USA: Paleogeographic implications: Sedimentary Geology, v. 163, p. 29–66 https://doi.org/10.1016/S0037-0738(03)00158-1.
- Dickinson, W.R., and Gehrels, G.E., 2008, Sediment delivery to the Cordilleran foreland basin: Insights from U-Pb ages of detrital zircons in Upper Jurassic and Cretaceous strata of the Colorado Plateau: American Journal of Science, v. 308, p. 1041–1082.
- Dickinson, W.R., and Gehrels, G.E., 2009a, U-Pb ages of detrital zircons in Jurassic eolian and associated sandstones of the Colorado plateau: Evidence for transcontinental dispersal and intraregional recycling of sediment: Geological Society of America Bulletin, v. 121, p. 408–433, https://doi.org/10.1130/B26406.1.
- Dickinson, W.R., and Gehrels, G.E., 2009b, Use of U-Pb ages of detrital zircons to infer maximum depositional ages of strata: A test against a Colorado Plateau Mesozoic database: Earth and Planetary Science Letters, v. 288, p. 115–125 https://doi.org/10.1016/j.epsl.2009.09.013.
- Dickinson, W.R., and Snyder, W.S., 1978, Plate tectonics of the Laramide orogeny, in Williams, V., III, ed., Laramide Folding Associated with Basement Block Faulting in the Western United States: Geological Society of America Memoir 151, p. 355–366, https://doi.org/10.1130/MEM151-p355.
- Dickinson, W.R., Klute, M.A., Hayes, M.J., Janecke, S.U., Lundin, E.R., McKittrick, M.A., and Olivares, M.D.,

- 1988, Paleogeographic and paleotectonic setting of Laramide sedimentary basins in the central Rocky Mountain region: Geological Society of America Buletin, v. 100, p. 1023–1039, https://doi.org/10.1130/0016-7606(1988)100<1023:PAPSOL>2.3.CO;2.
- Dickinson, W.R., Lawton, T.F., Pecha, M., Davis, S.J., Gehrels, G.E., and Young, R.A., 2012, Provenance of the Paleogene Colton Formation (Uinta Basin) and Cretaceous-Paleogene provenance evolution in the Utah foreland: Evidence from U-Pb ages of detrital zircons, paleocurrent trends, and sandstone petrofacies: Geosphere, v. 8, p. 854–880 https://doi.org/10 .1130/GES00763.1.
- Dott, R.H., Jr., 1964, Wacke, graywacke and matrix: What approach to immature sandstone classification?: Society of Economic Paleontologists and Mineralogists Journal of Sedimentary Research, v. 34, p. 625–632.
- Erslev, E.A., 1988, Normalized center-to-center strain analysis of packed aggregates: Journal of Structural Geology, v. 10, p. 201–209 https://doi.org/10.1016 /0191-8141(88)90117-4.
- Fan, M., and Dettman, D.L., 2009, Late Paleocene high Laramide ranges in northeast Wyoming: Oxygen isotope study of ancient river water: Earth and Planetary Science Letters, v. 286, p. 110–121, https://doi.org/10 .1016/j.epsl.2009.06.024.
- Fan, M., Hough, B.G., and Passey, B.H., 2014, Middle to late Cenozoic cooling and high topography in the central Rocky Mountains: Constraints from clumped isotope geochemistry: Earth and Planetary Science Letters, v. 408, p. 35–47, https://doi.org/10.1016/j.epsl.2014 .09.050.
- Fayon, A.K., Tikoff, B., Kahn, M., and Gaschnig, R.M., 2017, Cooling and exhumation of the southern Idaho batholith: Lithosphere, v. 9, p. 299–314 https://doi.org /10.1130/L565.1.
- Fedo, C.M., Sircombe, K.N., and Rainbird, R.H., 2003, Detrital zircon analysis of the sedimentary record: Reviews in Mineralogy and Geochemistry, v. 53, p. 277–303 https://doi.org/10.2113/0530277.
- Forss, C.D., 1983, Fluvial sediment dispersal and the infilling of Lake Gosiute (Eocene), Washakie Basin, Wyoming (Cathedral Bluffs Tongue, Wasatch Formation: Laney Member, Green River Formation): Columbus, Ohio, Ohio State University, http://rave.ohiolink.edu/etdc/view?acc_num=osu1380553429.
- Fouch, T.D., 1981, Distribution of rock types, lithologic groups, and interpreted depositional environments for some lower Tertiary and upper Cretaceous rocks from outcrops at Willow Creek-Indian Canyon through the subsurface of Duchesne and Altamont oil fields, southwest to north-central parts of the Uinta Basin, Utah: U.S. Geological Survey Oil and Gas Investigation Chart Report 81, Open-File Report 77-509, https://doi.org/10.3133/oc81.
- Gao, M., and Fan, M., 2018, Depositional environment, sediment provenance and oxygen isotope paleoaltimetry of the early Paleogene greater Green River Basin, Southwestern Wyoming, U.S.A: American Journal of Science, v. 318, p. 1018–1055.
- Gehrels, G., 2012, Detrital zircon U-Pb geochronology: Current methods and new opportunities, in Busby, C., and Azor, A., eds., Tectonics of Sedimentary Basins: Recent Advances: Oxford, UK, Blackwell Publishing, p. 45–62, https://doi.org/10.1002/9781444347166.ch2.
- Gehrels, G., 2014, Detrital zircon U-Pb geochronology applied to tectonics: Annual Review of Earth and Planetary Sciences, v. 42, p. 127–149 https://doi.org/10.1146/annurev-earth-050212-124012.
- Gehrels, G., and Pecha, M., 2014, Detrital zircon U-Pb geochronology and Hf isotope geochemistry of Paleozoic and Triassic passive margin strata of western North America: Geosphere, v. 10, p. 49–65, https://doi.org/10 .1130/GES00889.1.
- Gehrels, G.E., Valencia, V.A., and Ruiz, J., 2008, Enhanced precision, accuracy, efficiency, and spatial resolution of U-Pb ages by laser ablation-multicollector-inductively coupled plasma-mass spectrometry: Geochemistry, Geophysics, Geosystems, v. 9, https://doi.org/10.1029/ /2007GC001805.
- Gehrels, G.E., Blakey, R., Karlstrom, K.E., Timmons, J.M., Dickinson, B., and Pecha, M., 2011, Detrital zircon U-Pb geochronology of Paleozoic strata in the Grand

- Canyon, Arizona: Lithosphere, v. 3, p. 183–200, https://doi.org/10.1130/L121.1.
- Gonzales, D.A., 2015, New U-Pb Zircon and 40Ar/39Ar age constraints on the Late Mesozoic to Cenozoic plutonic record in the western San Juan Mountains: The Mountain Geologist, v. 52, p. 5–42 https://doi.org/10.31582 /rmag.mg.52.2.5.
- Grace, R.L., Chamberlain, K.R., Frost, B.R., and Frost, C.D., 2006, Tectonic histories of the Paleo- to Mesoarchean Sacawee block and Neoarchean Oregon Trail structural belt of the south-central Wyoming Province: Canadian Journal of Earth Sciences, v. 43, p. 1445–1466 https:// doi.org/10.1139/e06-083.
- Hammond, A.P., Carroll, A.R., Parrish, E.C., Smith, M.E., and Lowenstein, T.K., 2019, The Aspen paleoriver: Linking Eocene magnatism to the world's largest Nacarbonate evaporite (Wyoming, USA): Geology, v. 47, p. 1020–1024, https://doi.org/10.1130/G46419.1.
- Hansen, W.R., 1965, Geology of the Flaming Gorge Area, Utah-Colorado-Wyoming: U.S. Geological Survey Professional Paper 490, 196 p., https://doi.org/10.3133/pp490.
- Hinderer, M., and Einsele, G., 2001, The world's large lake basins as denudation-accumulation systems and implications for their lifetimes: Journal of Paleolimnology, v. 26, p. 355–372, https://doi.org/10.1023 /A:1012651232541.
- Honig, S., Carroll, A., Gygi, D., and Smith, M.E., 2020, Early Eocene drainage evolution of the Idaho paleoriver, Green River Basin, Wyoming [M.S. thesis]: Madison, Wisconsin, University of Wisconsin–Madison, 153 p.
- Horstwood, M.S.A., et al., 2016, Community-derived standards for LA-ICP-MS U-(Th-)Pb geochronology: Uncertainty propagation, age interpretation and data reporting: Geostandards and Geoanalytical Research, v. 40, p. 311–332 https://doi.org/10.1111/j.1751-908X.2016.00379.x.
- Ingersoll, R.V., Bullard, T.F., Ford, R.L., Grimm, J.P., Pickle, J.D., and Sares, S.W., 1984, The effect of grain size on detrital modes: A test of the Gazzi-Dickinson point-counting method (Holocene, sand, New Mexico, USA): Journal of Sedimentary Petrology, v. 54, p. 103–116.
- Jackson, L.J., Horton, B.K., and Vallejo, C., 2019, Detrital zircon U-Pb geochronology of modern Andean rivers in Ecuador: Fingerprinting tectonic provinces and assessing downstream propagation of provenance signals: Geosphere, v. 15, p. 1943–1957 https://doi.org/10.1130 /GES02126.1.
- Jesse, G., Ryder, R.T., Johnson, R.C., Brownfield, M.E., and Mercier, T.J., 2011, Stratigraphic cross sections of the Eocene Green River Formation in the Green River Basin, southwestern Wyoming, northwestern Colorado, and northeastern Utah: U.S. Geological Survey Digital Data Series DDS-69-DD, 11 p.
- Karlstrom, K., Hagadorn, J., Gehrels, G., Matthews, W., Schmitz, M., Madronich, L., Mulder, J., Pecha, M., Giesler, D., and Crossey, L., 2018, Cambrian Sauk transgression in the Grand Canyon region redefined by detrital zircons: Nature Geoscience, v. 11, p. 438–443 https://doi.org/10.1038/s41561-018-0131-7.
- Karlstrom, K.E., and Houston, R.S., 1984, The Cheyenne belt: Analysis of a Proterozoic suture in Southern Wyoming: Precambrian Research, v. 25, p. 415–446 https:// doi.org/10.1016/0301-9268(84)90012-3.
- Karlstrom, K.E., Flurkey, A.J., and Houston, R.S., 1983, Stratigraphy and depositional setting of the Proterozoic Snowy Pass Supergroup, southeastern Wyoming: Record of an early Proterozoic Atlantic-type cratonic margin: Geological Society of America Bulletin, v. 94, p. 1257–1274, https://doi.org/10.1130 /0016-7606(1983)94<1257:SADSOT>2.0.CO;2.
- Klein, T.L., Evans, K.V., and DeWitt, E.H., 2010, Geochronology database for central Colorado: U.S. Geological Survey Data Series 489, 13 p.
- Laskowski, A.K., Decelles, P.G., and Gehrels, G.E., 2013, Detrital zircon geochronology of Cordilleran retroarc foreland basin strata, western North America: Tectonics, v. 32, p. 1027–1048, https://doi.org/10.1002/tect 20065
- Lawton, T.F., 2019, Laramide sedimentary basins and sediment-dispersal systems, in Miall, A.D., ed., The

- Sedimentary Basins of the United States and Canada (second edition): Amsterdam, Netherlands, Elsevier, p. 529–557, https://doi.org/10.1016/B978-0-444-63895-3.00013-9.
- Lawton, T.F., Hunt, G.J., and Gehrels, G.E., 2010, Detrital zircon record of thrust belt unroofing in Lower Cretaceous synorogenic conglomerates, central Utah: Geology, v. 38, p. 463–466, https://doi.org/10.1130 //330684.1.
- Leary, R.J., et al., 2020, Provenance of Pennsylvanian–Permian sedimentary rocks associated with the Ancestral Rocky Mountains orogeny in southwestern Laurentia: Implications for continental-scale Laurentian sediment transport systems: Lithosphere, v. 12, p. 88–121 https://doi.org/10.1130/L1115.1.
- Leier, A.L., and Gehrels, G.E., 2011, Continental-scale detrital zircon provenance signatures in Lower Cretaceous strata, western North America: Geology, v. 39, p. 399– 402, https://doi.org/10.1130/G31762.1.
- Link, P.K., Fanning, C.M., and Beranek, L.P., 2005, Reliability and longitudinal change of detrital-zircon age spectra in the Snake River system, Idaho and Wyoming: An example of reproducing the bumpy barcode: Sedimentary Geology, v. 182, p. 101–142 https://doi.org/10.1016/j.sedgeo.2005.07.012.
- Longworth, B.E., Petsch, S.T., Raymond, P.A., and Bauer, J.E., 2007, Linking lithology and land use to sources of dissolved and particulate organic matter in headwaters of a temperate, passive-margin river system: Geochimica et Cosmochimica Acta, v. 71, p. 4233–4250 https:// doi.org/10.1016/j.gca.2007.06.056.
- Love, J.D., 1970, Cenozoic Geology of the Granite Mountains Area, Central Wyoming: U.S. Geological Survey Professional Paper 495-C, 154 p., https://doi.org/10.3133/pp495C.
- Love, J.D., McGrew, P.O., and Thomas, H.D., 1963, Relationship of the latest Cretaceous and Tertiary deposition and deformation to oil and gas in Wyoming, in Childs, O.E., and Beebe, B.W., eds., Backbone of the Americas: Tectonic History from Pole to Pole: AAPG Memoir 2, p. 1–13.
- Lynds, R.M., and Lichtner, D.T., 2016, Stratigraphy and hydrocarbon potential of the Fort Union and Lance Formations in the Great Divide and Washakie Basins, south-central Wyoming: Wyoming State Geological Survey Report of Investigations 73, 82 p., https://doi. org/10.13140/RG.2.1.4558.1040.
- Lynds, R.M., and Xie, X., 2019, Detrital zircon geochronology of Upper Cretaceous to Paleocene sandstones from south-central Wyoming: Evidence for middle Campanian Laramide deformation: Tectonics, v. 38, p. 4077–4098, https://doi.org/10.1029/2019TC005636.
- Ma, P., Wang, C., Meng, J., Ma, C., Zhao, X., Li, Y., and Wang, M., 2017, Late Oligocene-early Miocene evolution of the Lunpola Basin, central Tibetan Plateau, evidences from successive lacustrine records: Gondwana Research, v. 48, p. 224–236, https://doi.org/10.1016/j .gr.2017.04.023.
- Machlus, M.L., Ramezani, J., Bowring, S.A., Hemming, S.R., Tsukui, K., and Clyde, W.C., 2015, A strategy for cross-calibrating U-Pb chronology and astrochronology of sedimentary sequences: An example from the Green River Formation, Wyoming, USA: Earth and Planetary Science Letters, v. 413, p. 70–78, https://doi.org/10 .1016/j.epsl.2014.12.009.
- May, S.R., Gray, G.G., Summa, L.L., Stewart, N.R., Gehrels, G.E., and Pecha, M.E., 2013, Detrital zircon geochronology from the Bighorn Basin, Wyoming, USA: Implications for tectonostratigraphic evolution and paleogeography: Geological Society of America Bulletin, v. 125, p. 1403–1422, https://doi.org/10.1130/B30824.1
- Meyers, S.R., 2008, Resolving Milankovitchian controversies: The Triassic Latemar limestone and the Eocene Green River Formation: Geology, v. 36, p. 319–322 https://doi.org/10.1130/G24423A.1.
- Moecher, D., and Samson, S., 2006, Differential zircon fertility of source terranes and natural bias in the detrital zircon record: Implications for sedimentary provenance analysis: Earth and Planetary Science Letters, v. 247, p. 252–266 https://doi.org/10.1016/j.epsl.2006 .04.035.

- Mohrig, D., Heller, P.L., and Lyons, W.J., 2000, Interpreting avulsion process from ancient alluvial sequences: Guadalope-Matarranya system (northern Spain) and Wasatch Formation (western Colorado): Geological Society of America Bulletin, v. 112, p. 1787–1803, https://doi.org/10.1130/0016-7606(2000)112<1787: IAPFAA>2.0.CO;2.
- Murphy, E.M.A., and Salvador, A., 1999, International Stratigraphic Guide: An abridged version: Episodes, v. 22, p. 255–271, https://doi.org/10.18814/epiiugs/1999 /v22i4/002.
- Nesse, W.D., 2012, Introduction to Mineralogy: Oxford, UK, Oxford University Press, 480 p.
- Norton, K.P., von Blanckenburg, F., and Kubik, P.W., 2010, Cosmogenic nuclide-derived rates of diffusive and episodic erosion in the glacially sculpted upper Rhone Valley, Swiss Alps: Earth Surface Processes and Landforms, v. 35, p. 651–662 https://doi.org/10.1002/esp .1961.
- Otteman, A.S., and Snoke, A.W., 2005, Structural analysis of a Laramide, basement-involved, foreland fault zone, Rawlins uplift, south-central Wyoming: Rocky Mountain Geology, v. 40, p. 65–89, https://doi.org/10.2113 /40.1.65.
- Pecha, M.E., Gehrels, G.E., Karlstrom, K.E., Dickinson, W.R., Donahue, M.S., Gonzales, D.A., and Blum, M.D., 2018, Provenance of Cretaceous through Eocene strata of the Four Corners region: Insights from detrital zircons in the San Juan Basin, New Mexico and Colorado: Geosphere, v. 14, p. 785–811, https://doi.org/10 .1130/GES01485.1.
- Picard, M.D., Bruhn, R.L., and Beck, S.L., 1983, Mesozoic and Early Tertiary paleostructure and sedimentology of central Wasatch Mountains, Uinta Mountains, and Uinta Basin [abstract]: AAPG Bulletin, v. 67, p. 63– 105 https://doi.org/10.1306/03B5B95C-16D1-11D7 -8645000102C1865D.
- Pietras, J.T., and Carroll, A.R., 2006, High-resolution stratigraphy of an underfilled lake basin: Wilkins Peak Member, Eocene Green River Formation, Wyoming, U.S.A: Journal of Sedimentary Research, v. 76, p. 1197–1214, https://doi.org/10.2110/jsr.2006.096.
- Pipiringos, G.N., and Denson, N.M., 1970, The Battle Spring Formation in south-central Wyoming, in Enyert, R.L., et al., eds., Wyoming Geological Association, 22nd Annual Field Conference Guidebook, 1970: Symposium on Wyoming Sandstones, Their Economic Importance: Past, Present and Future: Casper, Wyoming, Wyoming Geological Association, p. 161–168.
- Por, F.D., 2000, The Pantanal (Mato Grosso, Brazil) and other "hemiendorheic" basins: Paradigms for their preservation: SIL Proceedings, 1922–2010, v. 27, p. 752–755, https://doi.org/10.1080/03680770.1998.11901335.
- Premo, W.R., and Van Schmus, W.R., 1989, Zircon geochronology of Precambrian rocks in southeastern Wyoming and northern Colorado, in Grambling, J.A., and Tewksbury, B.J., eds., Proterozoic Geology of the Southern Rocky Mountains: Geological Society of America Special Paper 235, p. 13–32 https://doi.org/10.1130 /SPE235-p13.
- Pullen, A., Ibáñez-Mejía, M., Gehrels, G.E., Ibáñez-Mejía, J.C., and Pecha, M., 2014, What happens when n = 1000?: Creating large-n geochronological datasets with LA-ICP-MS for geologic investigations: Journal of Analytical Atomic Spectrometry, v. 29, p. 971–980 https://doi.org/10.1039/C4JA00024B.
- Pullen, Å., Ibáñez-Mejia, M., Gehrels, G.E., Giesler, D., and Pecha, M., 2018, Optimization of a laser ablation-single collector-inductively coupled plasma-mass spectrometer (Thermo Element 2) for accurate, precise, and efficient zircon U-Th-Pb geochronology: Geochemistry, Geophysics, Geosystems, v. 19, p. 3689–3705 https:// doi.org/10.1029/2018GC007889.
- Rainbird, R., Cawood, P., and Gehrels, G., 2012, The great Grenvillian sedimentation episode: Record of supercontinent Rodinia's assembly, in Busby, C., and Azor, A., eds., Tectonics of Sedimentary Basins: Recent Advances: Oxford, UK, Blackwell Publishing, p. 583– 601, https://doi.org/10.1002/9781444347166.ch29.
- Rhodes, M.K., and Carroll, A.R., 2015, Lake type transition from balanced-fill to overfilled: Laney Member, Green River Formation, Washakie Basin, Wyoming, in Smith,

- M.E., and Carroll, A.R., eds., Stratigraphy and Paleolimnology of the Green River Formation, Western USA: Dordrecht, Netherlands, Springer, v. 1, p. 103–125, https://doi.org/10.1007/978-94-017-9906-5_5.
- Roehler, H.W., 1969, Stratigraphy and oil-shale deposits of Eocene rocks in the Washakie Basin, Wyoming: Wyoming Geological Association, 21st Annual Field Conference Guidebook, v. 21, p. 197–206.
- Roehler, H.W., 1992, Correlation, Composition, Areal Distribution, and Thickness of Eocene Stratigraphic Units, Greater Green River Basin, Wyoming, Utah, and Colorado: U.S. Geological Survey Professional Paper 1506-E, 49 p., https://doi.org/10.3133/pp1506E.
- Roehler, H.W., 1993, Eocene Climates, Depositional Environments, and Geography, Greater Green River Basin, Wyoming, Utah, and Colorado: U.S. Geological Survey Professional Paper 1506-F, 74 p., https://doi.org/10.3133/pp1506F.
- Romans, B.W., Castelltort, S., Covault, J.A., Fildani, A., and Walsh, J.P., 2016, Environmental signal propagation in sedimentary systems across timescales: Earth-Science Reviews, v. 153, p. 7–29, https://doi.org/10 .1016/j.earscirev.2015.07.012.
- Saylor, J.E., and Sundell, K.E., 2016, Quantifying comparison of large detrital geochronology data sets: Geosphere, v. 12, p. 203–220 https://doi.org/10.1130/GES01237.1.
- Saylor, J.E., Jordan, J.C., Sundell, K.E., Wang, X., Wang, S., and Deng, T., 2018, Topographic growth of the Jishi Shan and its impact on basin and hydrology evolution, NE Tibetan Plateau: Basin Research, v. 30, p. 544–563, https://doi.org/10.1111/bre.12264.
- Schneider, S., Hornung, J., and Hinderer, M., 2016, Evolution of the western East African Rift System reflected in provenance changes of Miocene to Pleistocene synrift sediments (Albertine Rift, Uganda): Sedimentary Geology, v. 343, p. 190–205, https://doi.org/10.1016/j.sedgeo.2016.07.013.
- Sharman, G.R., Sharman, J.P., and Sylvester, Z., 2018, detritalPy: A Python-based toolset for visualizing and analysing detrital geo-thermochronologic data: The Depositional Record: A Journal of Biological, Physical and Geochemical Sedimentary Processes, v. 4, p. 202–215 https://doi.org/10.1002/dep2.45.
- Sickmann, Z.T., Paull, C.K., and Graham, S.A., 2016, Detrital-zircon mixing and partitioning in fluvial to deep marine systems, central California, U.S.A: Journal of Sedimentary Research, v. 86, p. 1298–1307, https://doi.org/10.2110/jsr.2016.78.
- Sircombe, K.N., and Stern, R.A., 2002, An investigation of artificial biasing in detrital zircon U-Pb geochronology due to magnetic separation in sample preparation: Geochimica et Cosmochimica Acta, v. 66, p. 2379–2397 https://doi.org/10.1016/S0016 -7037(02)00839-6.
- Smith, M.E., Singer, B., and Carroll, A., 2003, 40Ar/39Ar geochronology of the Eocene Green River Formation, Wyoming: Geological Society of America Bulletin, v. 115, p. 549–565 https://doi.org/10.1130/0016-7606(2003)115
- Smith, M.E., Carroll, A.R., and Singer, B.S., 2008, Synoptic reconstruction of a major ancient lake system: Eocene Green River Formation, western United States: Geological Society of America Bulletin, v. 120, p. 54–84 https://doi.org/10.1130/B26073.1.
- Smith, M.E., Chamberlain, K.R., Singer, B.S., and Carroll, A.R., 2010, Eocene clocks agree: Coeval 40Ar/39Ar, U-Pb, and astronomical ages from the Green River Formation: Geology, v. 38, p. 527–530 https://doi.org/10 .1130/G30630.1.
- Smith, M.E., Carroll, A.R., Scott, J.J., and Singer, B.S., 2014, Early Eocene carbon isotope excursions and landscape destabilization at eccentricity minima: Green River Formation of Wyoming: Earth and Planetary Science Letters, v. 403, p. 393–406, https://doi.org//10.1016/j .epsl.2014.06.024.
- Smith, M.E., Carroll, A.R., and Scott, J.J., 2015, Stratigraphic expression of climate, tectonism, and geomorphic forcing in an underfilled lake basin: Wilkins Peak Member of the Green River Formation, in Smith, M.E., and Carroll, A.R., eds., Stratigraphy and Paleolimnology of the Green River Formation, Western USA: Dordrecht,

- Netherlands, Springer, v. 1, p. 61–102, https://doi.org/10.1007/978-94-017-9906-5_4.
- Smoot, J.P., 1983, Depositional subenvironments in an arid closed basin; the Wilkins Peak Member of the Green River Formation (Eocene), Wyoming, U.S.A: Sedimentology, v. 30, p. 801–827 https://doi.org/10.1111/j .1365-3091.1983.tb00712.x.
- Souders, A.K., and Frost, C.D., 2006, In suspect terrane?: Provenance of the late Archean Phantom Lake metamorphic suite, Sierra Madre, Wyoming: Canadian Journal of Earth Sciences, v. 43, p. 1557–1577 https://doi.org/10.1139/e06-114.
- Stahl, M., Wassik, J., Gehring, J., Horan, C., and Wozniak, A., 2021, Connecting the age and reactivity of organic carbon to watershed geology and land use in tributaries of the Hudson River: Journal of Geophysical Research: Biogeosciences, v. 126, no. 9, https://doi.org/10.1029 /2021JG006494.
- Sullivan, R., 1980, Stratigraphic evaluation of the Eocene rocks of southwestern Wyoming: Geological Survey of Wyoming Report of Investigations 20, 50 p.
- Sullivan, R., 1985, Origin of lacustrine rocks of Wilkins Peak Member, Wyoming: AAPG Bulletin, v. 69, p. 913–922 https://doi.org/10.1306/AD462B1E-16F7-11D7 -8645000102C1865D.
- Sundell, K.E., and Saylor, J.E., 2017, Unmixing detrital geochronology age distributions: Geochemistry, Geophysics, Geosystems, v. 18, p. 2872–2886 https://doi.org/10 .1002/2016GC006774.
- Surdam, R.C., and Stanley, K.O., 1980, Effects of changes in drainage-basin boundaries on sedimentation in Eocene Lakes Gosiute and Uinta of Wyoming, Utah and Colorado: Geology, v. 8, p. 135–139 https://doi.org/10.1130 /0091-7613(1980)8<135:EOCIDB>2.0.CO;2.

- Templeton, M.E., and Smithson, S.B., 1994, Seismic reflection profiling of the Cheyenne belt Proterozoic suture in the Medicine Bow Mountains, southeastern Wyoming: A tie to geology: Tectonics, v. 13, p. 1231–1241, https:// doi.org/10.1029/94TC00626.
- Tweto, O., and Sims, P.K., 1963, Precambrian ancestry of the Colorado mineral belt: Geological Society of America Bulletin, v. 74, p. 991–1014 https://doi.org/10.1130 /0016-7606(1963)74[991:PAOTCM]2.0.CO;2.
- Vermeesch, P., 2013, Multi-sample comparison of detrital age distributions: Chemical Geology, v. 341, p. 140–146 https://doi.org/10.1016/j.chemgeo.2013.01.010.
- Vermeesch, P., 2018, Dissimilarity measures in detrital geochronology: Earth-Science Reviews, v. 178, p. 310–321 https://doi.org/10.1016/j.earscirev.2017 .11.027.
- Weimer, R.J., 1960, Upper Cretaceous Stratigraphy, Rocky Mountain Area: AAPG Bulletin, v. 44, p. 1–20 https://doi.org/10.1306/0BDA5F6F-16BD-11D7 -8645000102C1865D.
- Weissmann, G.S., Hartley, A.J., Nichols, G.J., Scuderi, L.A., Olson, M., Buehler, H., and Banteah, R., 2010, Fluvial form in modern continental sedimentary basins: Distributive fluvial systems: Geology, v. 38, p. 39–42 https://doi.org/10.1130/G30242.1.
- Weissmann, G.S., Hartley, A.J., Scuderi, L.A., Nichols, G.J., Owen, A., Wright, S., Felicia, A.L., Holland, F., and Anaya, F.M.L., 2015, Fluvial geomorphic elements in modern sedimentary basins and their potential preservation in the rock record: A review: Geomorphology, v. 250, p. 187–219 https://doi.org/10.1016/j.geomorph .2015.09.005.
- West, A.J., Bickle, M.J., Collins, R., and Brasington, J., 2002, Small-catchment perspective on Himalayan weather-

- ing fluxes: Geology, v. 30, p. 355–358 https://doi.org/10.1130/0091-7613(2002)030<0355:SCPOHW>2.0.CO:2.
- Whitmeyer, S.J., and Karlstrom, K.E., 2007, Tectonic model for the Proterozoic growth of North America: Geosphere, v. 3, p. 220–259 https://doi.org/10.1130 /GES00055.1.
- Wren, D.G., and Davidson, G.R., 2011, Using lake sedimentation rates to quantify the effectiveness of erosion control in watersheds: Journal of Soil and Water Conservation, v. 66, p. 313–322 https://doi.org/10.2489/jswc.66.5.313.
- Yonkee, W.A., Dehler, C.D., Link, P.K., Balgord, E.A., Keeley, J.A., Hayes, D.S., Wells, M.L., Fanning, C.M., and Johnston, S.M., 2014, Tectono-stratigraphic framework of Neoproterozoic to Cambrian strata, west-central U.S.: Protracted rifting, glaciation, and evolution of the North American Cordilleran margin: Earth-Science Reviews, v. 136, p. 59–95, https://doi .org/10.1016/j.earscirev.2014.05.004.
- Zhao, G., Klik, A., Mu, X., Wang, F., Gao, P., and Sun, W., 2015, Sediment yield estimation in a small watershed on the northern Loess Plateau, China: Geomorphology, v. 241, p. 343–352 https://doi.org/10.1016/j.geomorph 2015.04.020.

SCIENCE EDITOR: WENJIAO XIAO ASSOCIATE EDITOR: DANIEL PEPPE

MANUSCRIPT RECEIVED 27 OCTOBER 2022 REVISED MANUSCRIPT RECEIVED 24 MAY 2023 MANUSCRIPT ACCEPTED 5 JULY 2023

Printed in the USA